Chemical Science

ROYAL SOCIETY OF CHEMISTRY

REVIEW

View Article Online
View Journal | View Issue

Cite this: *Chem. Sci.*, 2026, **17**, 7376

Delicate molecular design, self-assembly and functional applications of chiral cyclophanes

Yiming Zhang, [a] Hongzhe Jia,[a] Lijin Xu, *[a] Minghua Liu [b] and Guanghui Ouyang *[a]

Chiral cyclophanes represent a unique supramolecular architecture that integrates chiral cavities with luminescent properties, enabled by their precisely controlled interchromophoric orientation, distance, and asymmetry. These features confer exceptional chiral recognition capabilities and distinctive chiroptical behaviors. Over the past decade, advances in synthetic strategies alongside improved computational and analytical tools, have greatly accelerated the development of diverse chiral cyclophane structures and deepened mechanistic understanding. Currently, the field is demonstrating expanding functionalities, showing significant promise in areas such as circularly polarized luminescence, asymmetric catalysis, supramolecular assembly, and biomedicine. This review systematically summarizes recent progress in chiral cyclophanes, offering a timely overview of the historical context, current achievements, and future directions. Based on the location of chiral elements and overall molecular geometry, the discussed cyclophanes are categorized into four subtypes: those containing chiral chromophores, those with chiral linkers, systems exhibiting planar chirality, and chiral cyclophanes with stacked multilayer chromophores. By organizing the literature according to these structural classes, this review aims to offer clear guidance for the rational design and functional exploration of chiral cyclophanes, thereby fostering interdisciplinary innovation across chemistry, materials science, life sciences and other related fields.

Received 18th December 2025
Accepted 10th March 2026

DOI: 10.1039/d5sc09932c

rsc.li/chemical-science

1. Introduction

Cyclophanes are a class of macrocyclic molecules consisting of aromatic structural units and suitable linkers.[1] Their unique structures have granted them a pivotal role in the history of supramolecular chemistry. They are regarded, alongside crown ethers,[2,3] cyclodextrins,[4–6] and calixarenes,[7–9] as foundational macrocyclic host molecules. A key feature of many cyclophanes is their inherently preorganized cavity between face-to-face

[a]*School of Chemistry and Life Resources, Renmin University of China, No. 59 Zhongguancun Street, Haidian District, Beijing, 100872, China. E-mail: ouyanggh@ruc.edu.cn; 20050062@ruc.edu.cn*

[b]*CAS Key Laboratory of Colloid, Interface and Thermodynamics, Institute of Chemistry, Chinese Academy of Sciences, North First Street 2, Zhongguancun, Beijing, 100190, China*

Yiming Zhang

Yiming Zhang received his bachelor's degree from Zhejiang University in 2021 and his master's degree from the same university in 2024. He is currently a PhD candidate under the supervision of Prof. Lijin Xu and Prof. Guanghui Ouyang at the School of Chemistry and Life Resources, Renmin University of China. His research focuses on the synthesis and self-assembly of chiral supramolecular structures.

Hongzhe Jia

Hongzhe Jia completed his undergraduate studies at Qingdao University of Science and Technology, and has been pursuing his postgraduate studies at the School of Chemistry and Life Resources, Renmin University of China since 2024, under the supervision of Prof. Lijin Xu and Prof. Guanghui Ouyang. His research interest focuses on the self-assembly of organic small molecules.

arranged chromophores, which facilitates efficient molecular recognition and has laid the groundwork for host–guest chemistry.[10–12] Cyclophane chemistry began in the mid-20th century with the discovery and synthesis of [2.2] paracyclophane(PCP).[13–15] Subsequently, advances and innovations in synthetic methodologies led to the emergence of various new types of cyclophanes, such as heteroatom-containing cyclophanes and cationic cyclophanes.[1,16,17] The study of these novel structures has significantly broadened the functional scope and applications of cyclophane chemistry. For example, tetraazacyclophanes can serve as artificial enzyme mimics, enabling biomolecular recognition and enzyme function simulation.[18,19] Tetracationic cyclophanes, such as $CBPQT^{4+}$ and its derivatives, have become a research focus in molecular machines and functional materials due to their controllable photochemical and electrochemical properties.[20,21] These examples together show the great potential of cyclophanes as a molecular platform with a tunable structure and diverse functions.

Chirality, a core concept in organic chemistry,[22] describes the geometric property of a molecule that is non-superimposable on its mirror image. Since the discovery of molecular chirality during the separation of tartaric acid, chiral molecules have gained widespread attention.[23–26] Molecular chirality can be categorized into several main types. These include central chirality (around a central atom which is bonded to multiple different substituents), axial chirality (*e.g.*, in allene and binaphthyl), planar chirality (*e.g.*, in *E*-cyclooctene or substituted PCP where rotation of *a* plane is restricted), and helical chirality (as seen in a molecule which has a helical structure, such as left- or right-handed helicenes).[27] Chirality not only describes the structural dissymmetry, but also leads to many unique functions. Chiral molecules are typically optically active. Moreover, structures with specific chromophores or luminescent moieties can exhibit properties like circular dichroism (CD)[28–30] and circularly polarized luminescence (CPL).[31,32] Consequently, chirality has extensive applications in fields such as materials science,[33–35] biochemistry,[36–38] and pharmaceuticals.[39–41]

Integrating chirality into cyclophanes creates a synergistic architecture: the well-defined, preorganized cavity of the cyclophane amplifies and expresses chiral information, while the introduced chirality directs host–guest interactions and chiroptical properties.[42,43] In this context, such a confined space is often referred to as a "chiral cavity", which describes a cavity that provides an effectively chiral environment for guest molecules. Importantly, the chirality of the cavity may arise either from an intrinsically asymmetric cavity geometry or from the surrounding chiral framework, even when the cavity itself is formally symmetric. This combination, achieved through precise control over interchromophoric orientation, distance, and asymmetry, enables exceptional chiral recognition and

Lijin Xu

Lijin Xu was born and brought up in Shandong, China. He studied chemistry at Qufu Normal University, and received in 1998, a PhD degree from the Institute of Chemistry, the Chinese Academy of Sciences. During 1998–2000, he held a two-year postdoctoral fellowship at the Leverhulme Centre for Innovative Catalysis, the University of Liverpool under the direction of Prof. Jianliang Xiao. After a one-year postdoctoral appointment in Loughborough University, he joined Prof. Albert S. C. Chan's group as a research associate in The Hong Kong Polytechnic University. In 2005, he took up an Associate Professor position in Department of Chemistry, Renmin University of China, and was promoted to full professor in 2010. His research interest mainly includes asymmetric catalysis, synthetic methodology, and green chemistry.

Minghua Liu

Minghua Liu graduated from Nanjing University in 1986. He received his PhD from Saitama University, Japan in 1994. After doing postdoctoral research at the Institute of Physical and Chemical Research (RIKEN) and at the Tokyo University of Agriculture and Industry, he joined the Institute of Photographic Chemistry in 1998 and then the Institute of Chemistry, CAS in 1999 and has been working as a professor to date. His research interests cover supramolecular chemistry, colloid and interface science, self-assembly and gel-based soft nanomaterials.

Guanghui Ouyang

Guanghui Ouyang was born in Hunan Province, China. He earned his BSc from the University of Science and Technology of China (USTC) in 2010 and his PhD from the Institute of Chemistry, Chinese Academy of Sciences (ICCAS) in 2015. From 2015 to 2025, he worked at ICCAS, where he advanced from assistant professor to associate professor and professor. Since 2025, he has been a full professor at Renmin University of China. His research interests include the synthesis of chiral π-conjugated molecules, self-assembled chiral nanostructures, supramolecular gels and chiroptical materials.

distinct optical behaviors such as strong circularly polarized luminescence and optical asymmetry.[44,45] The field of chiral cyclophanes is now at a pivotal stage. Synthetic methods including dynamic covalent chemistry and metal catalysis have matured, allowing more efficient and diverse constructions. Meanwhile, advances in computational and analytical tools are shifting the focus from structural exploration toward mechanistic understanding. Most importantly, chiral cyclophanes are demonstrating expanding functionality, showing great promise in areas such as CPL materials, chiral sensing, and asymmetric catalysis.

Although several insightful reviews have summarized progress in chiral macrocycles, few have focused specifically on cyclophane-based systems and their unique chiral functions. Therefore, a dedicated and systematic review of chiral cyclophanes is both timely and necessary. This review will adopt a structure-based classification organized by the origin of chirality, such as π-system chirality, linker chirality, and planar chirality, to provide a logical framework for understanding and designing these molecules. By comprehensively discussing their diverse structures, properties, and applications, this work aims to fill existing gaps in the literature and offer forward-looking perspectives to guide future research in this dynamic interdisciplinary field. It is worth noting that the scope of this review is not limited to cyclophanes in the strict classical sense, but also encompasses some macrocyclic compounds with cyclophane-like structural features. Although these systems do not strictly fall within the traditional definition of cyclophanes, they share key characteristics such as confined cavities, spatial organization of aromatic units, and the resulting chiral features and chiroptical responses. Therefore, inclusion of these structures enables a broader perspective for summarizing the design principles and functional applications of such chiral macrocyclic systems.

2. Molecular structure and synthesis of chiral cyclophanes

The chirality of cyclophanes, unlike that of simple small molecules, can originate from multiple structural elements within their macrocyclic framework. This complexity provides a clear rationale for a systematic classification. Following the framework introduced earlier, this chapter will systematically categorize chiral cyclophanes into four major classes based on their origin of chirality (Scheme 1): (i) chirality from π-systems, (ii) chirality from linkers, (iii) planar chirality, and (iv) multilayer chiral cyclophanes. For each category, we will examine in detail the representative structures, stereochemical features, and key synthetic strategies, aiming to elucidate how the origin of chirality guides the design and construction of these functional molecules.

2.1 Cyclophanes with chirality from π-systems

This category includes chiral cyclophanes whose asymmetry primarily originates from their aromatic structural units, which represent one of the most important sources of chirality in these

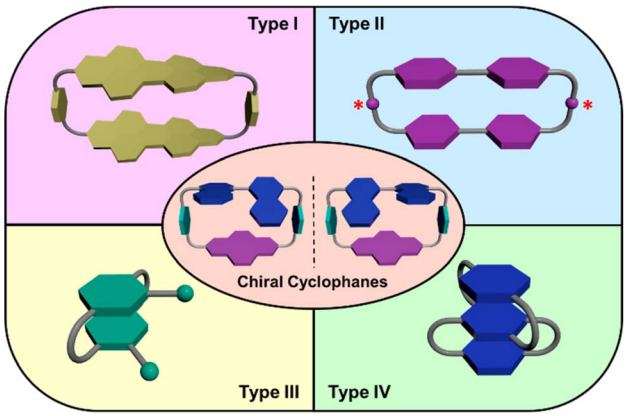

Scheme 1 Schematic classification of chiral cyclophanes: (i) chirality from the π-system, (ii) chirality from the linker (stereogenic carbon atoms indicated by red asterisks), (iii) planar chirality, and (iv) multilayer chiral cyclophanes.

macrocycles. These molecules can be further divided into two scenarios based on the mechanism of chirality generation. First, cyclophanes are constructed from inherently chiral aromatic units (*e.g.*, binaphthyls and helicenes), where the chirality is integrated into the macrocyclic framework and is transmitted throughout the entire structure. Second, the construction of the cyclophane locks the rapidly interconverting chiral conformations of aromatic units (*e.g.*, perylene diimides) that exist in the free state, resulting in stable and separable cyclophane enantiomers.

1,1′-Bi-2-naphthol (BINOL) is a classic axially chiral aromatic unit. Its configuration is stable and readily modifiable, making it widely used in the construction of not only chiral compounds,[46,47] but also an excellent building block for synthesizing chiral cyclophanes.[48] Reported cyclophane systems incorporating BINOL have shown a range of functionalities in areas such as chiral recognition, fluorescence sensing, and biological activity.[49–55] For instance, embedding the BINOL scaffold into cyclophane structures enables enantioselective recognition of pharmaceutical molecules[50] (*e.g.*, naproxen derivatives) and amino acids.[51,55] Some systems also hold promise in anion recognition and antibacterial applications.[53,54] These achievements fully illustrate the versatility and adaptability of BINOL as a chiral scaffold for constructing functionalized cyclophanes.

In recent years, research on BINOL-based chiral cyclophanes has increasingly focused on their cutting-edge optical properties and molecular recognition capabilities, leading to the emergence of diverse novel structures and applications. Takaishi *et al.* accessed a cyclophane **(*R*,*R*)-1** with D_2 symmetry, constructed from alternating, pyrene and binaphthyl units linked by ether bonds (Fig. 1a).[56] This molecule exhibits strong CPL with a high luminescence dissymmetry factor ($|g_{lum}| = 0.053$). Subsequently, the team replaced the ether linkages with thioether bonds (Fig. 1b),[57] which allows for dynamic modulation of its CPL properties by introducing conformational flexibility to the cyclophane. The CPL signal of this cyclophane

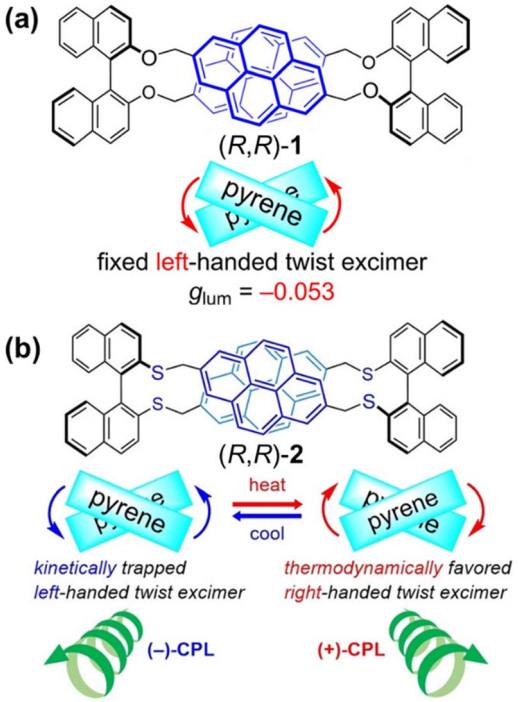

Fig. 1 Structures of chiral cyclophanes: (a) (*R*,*R*)-**1** containing ether linkages. Reproduced from ref. 56. Copyright 2022 Wiley-VCH; (b) (*R*,*R*)-**2** containing thioether linkages. Reproduced from ref. 57. Copyright 2024 Wiley-VCH.

shows temperature-induced sign inversion. This unique phenomenon stems from excited-state dynamics: at low temperatures, two pyrene units form a kinetically controlled left-handed twisted excimer, while at elevated temperatures, they transform into the thermodynamically more stable right-handed twisted excimer. This series of studies demonstrates the great potential of BINOL-based cyclophanes for developing high-performance CPL materials and stimulus-responsive CPL switches.

In a different approach, Stoddart and colleagues devised and synthesized a class of tetracationic cyclophanes, **(*RR*)/(*SS*)-$^{6,6'}$BinBox**·4PF$_6$, by embedding chiral binaphthyl fluorophores into pyridinium-based macrocycles (Fig. 2a).[58] Single-crystal X-ray diffraction analysis revealed that **(*SS*)-$^{6,6'}$BinBox**·4PF$_6$ adopts unique Figure-eight and square-like geometry (Fig. 2b). Most importantly, this molecule simultaneously achieves aggregation-induced emission (AIE) and CPL. Its AIE characteristics originate from restricted torsional motion of the chiral axis in the aggregated state, while CPL is maintained in both solution and aggregated states. The integration of AIE and CPL within a single BINOL-based cyclophane showcases their considerable promise for future optoelectronic and biological applications.

Furthermore, the prospect of chiral cyclophanes containing biphenyl units in enantioselective recognition has been extensively explored. Kinbara and colleagues designed and synthesized a series of multiblock amphiphilic cyclophanes ($\mathbf{C}_{SS}$, $\mathbf{C}_{RR}$ and $\mathbf{C}_{SR}$) incorporating biphenyl units (Fig. 3).[59] These

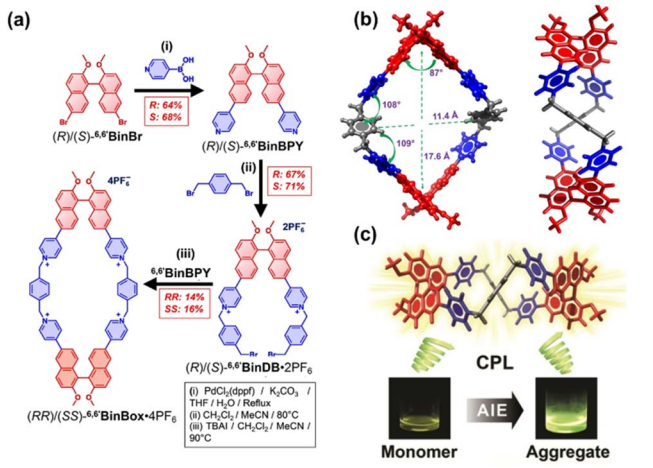

Fig. 2 (a) Synthesis of tetracationic cyclophane **(*RR*)/(*SS*)-$^{6,6'}$BinBox**·4PF$_6$; (b) Top and side views of **(*SS*)-$^{6,6'}$BinBox**·4PF$_6$; (c) Schematic illustration of the circularly polarized luminescence (CPL) and aggregation-induced emission (AIE) properties of **(*SS*)-$^{6,6'}$BinBox**·4PF$_6$. Reproduced from ref. 58. Copyright 2022 Wiley-VCH.

cyclophanes form aggregates in aqueous environments, with the biphenyl units in the homochiral $\mathbf{C}_{SS}$ and $\mathbf{C}_{RR}$ adopting more planar conformations compared to $\mathbf{C}_{SR}$. This distinct conformational preference underscores the pivotal role of the cyclophane framework in homochiral recognition and manifests its capability for enantioselective recognition, offering new design concepts for developing novel chiral sensing and separation materials operating in aqueous media.

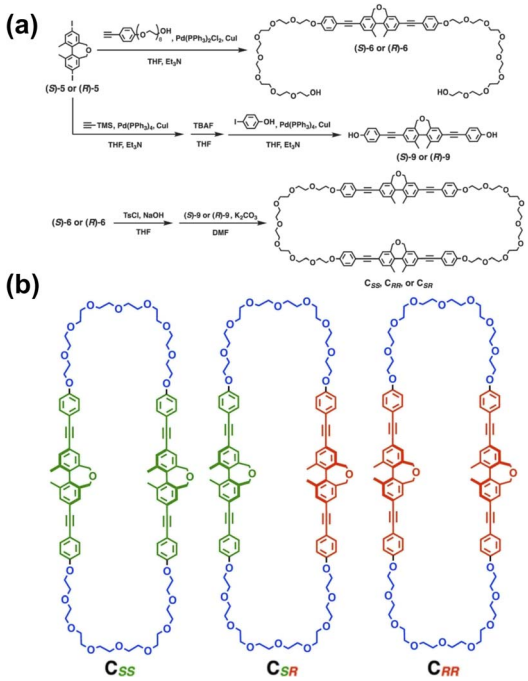

Fig. 3 Synthesis (a) and structures (b) of multiblock amphiphilic cyclophanes C_{SS}, C_{RR}, and C_{SR}. Reproduced from ref. 59. Copyright 2023 The Society of Polymer Science, Japan.

These examples illustrate that when axially chiral aromatic units such as BINOL are directly embedded as the π-core of cyclophane frameworks, the resulting chirality can be regarded as intrinsic to the π-system itself. In such cases, the aromatic unit not only provides structural rigidity but also directly contributes to the optical properties and chiroptical responses of the macrocycle. Nevertheless, in many other cyclophane systems, axially chiral aromatic motifs function primarily as connecting units between larger π frameworks, where chirality arises from the linker rather than from the main π-conjugated core. Such cases are discussed in the following section.

Perylene bisimides (PBI) are outstanding luminophores characterized by high fluorescence quantum yield and excellent stability. The introduction of substituents at the bay positions induces a twisted molecular core, conferring inherent conformational chirality. When PBI units are incorporated into cyclophane frameworks, the dynamic equilibrium between their (*M*) and (*P*) isomers becomes effectively constrained, leading to the formation of macrocyclic structures with chiral cavities.[60,61] These PBI-based chiral cyclophanes exhibit efficient energy transfer properties arising from the precise spatial arrangement of donor–acceptor pairs, as well as the capacity for chiral transmission and enantioselective recognition in host–guest chemistry due to their unique cavity architectures. These attributes underscore their strong prospects for applications in supramolecular chiroptics and sensing.

The Würthner group has conducted in-depth studies on chiral cyclophane systems containing PBI units, exploring their unique properties in molecular recognition and chirality regulation. They first reported a cyclophane **3** composed of two atropisomeric PBI units (Fig. 4a).[62] Variable-temperature NMR studies revealed a dynamic equilibrium among its three isomers [(*M*,*M*), (*P*,*P*), and (*M*,*P*)] at elevated temperatures. The non-chiral guest perylene preferentially binds to the homochiral (***M*,*M***)- and (***P*,*P***)-**3** over the heterochiral mesomer (***M*,*P***)-**3**. More importantly, when interacting with chiral guest molecules, the cyclophane exhibits a distinct preference for the homochiral (***M*,*M***) and (***P*,*P***)-**3** isomers (Fig. 4b). This work revealed for the first time that PBI-based cyclophanes can act as chiral hosts to receive and amplify chiral information through host–guest binding. Subsequently, by introducing bulkier substituents at the bay positions, they obtained PBI cyclophanes (**4-*PP*** and **4-*MM***, the heterochiral **4-*PM*** isomer was sterically forbidden) (Fig. 4c).[63] Contrary to expectations, this cyclophane did not follow the common "homochiral recognition" convention but instead showed a significant binding preference for heterochiral [5]helicene over its homochiral counterpart, with a nearly 5-fold difference in binding constants. Through density functional theory (DFT) calculations and single-crystal structure analysis, it was elucidated that this anomalous phenomenon stems from the substantial steric hindrance generated by the bay-position substituents of the cyclophane. This steric clash with homochiral guests compels the system to favor the formation of sterically more favorable heterochiral host–guest complexes (Fig. 4d). This conclusion can be extended to other aromatic guests with inherent conformational flexibility, leading to the proposal of a new

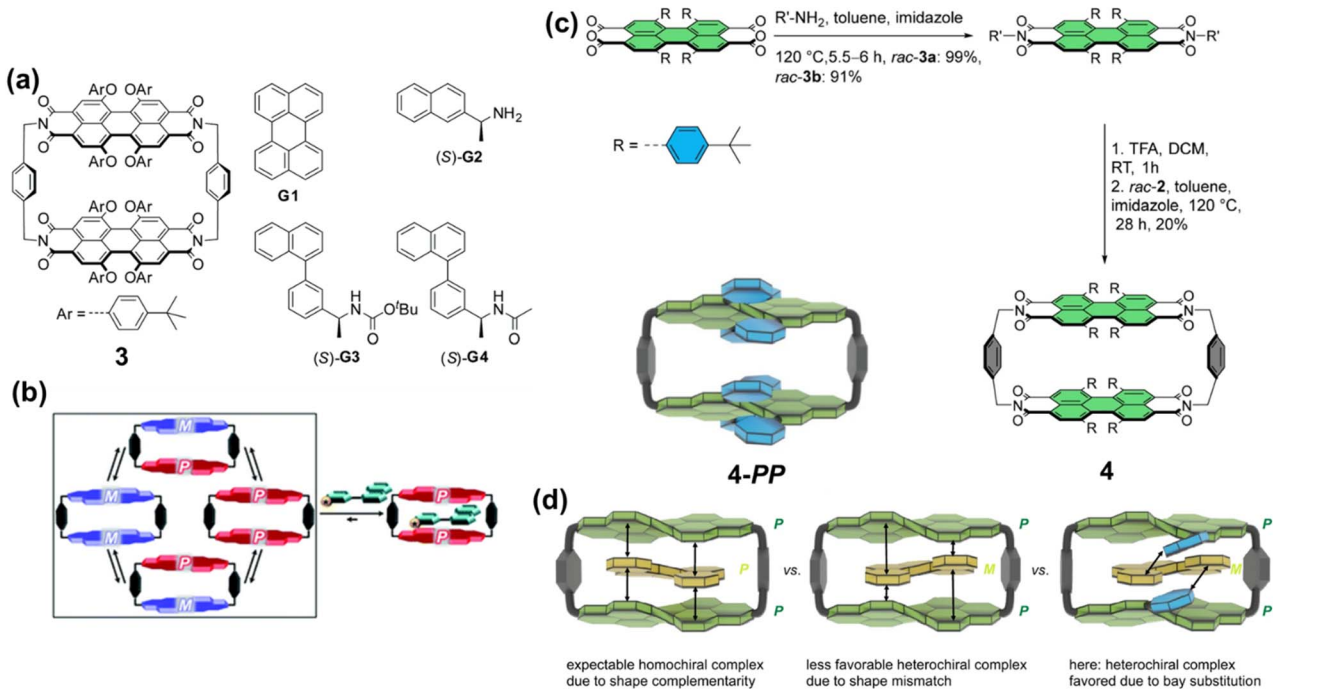

Fig. 4 (a) Structure of the bis-PBI cyclophane **3** and guest molecules; (b) Schematic illustration of the conformational equilibrium among the stereoisomers of **3**. Reproduced from ref. 62. Copyright 2019 Royal Society of Chemistry. (c) Synthesis of the PBI cyclophane **4**; (d) Formation of the host–guest complex between **4-*PP*** and a heterochiral guest. Reproduced from ref. 63. Copyright 2023 Springer-Nature.

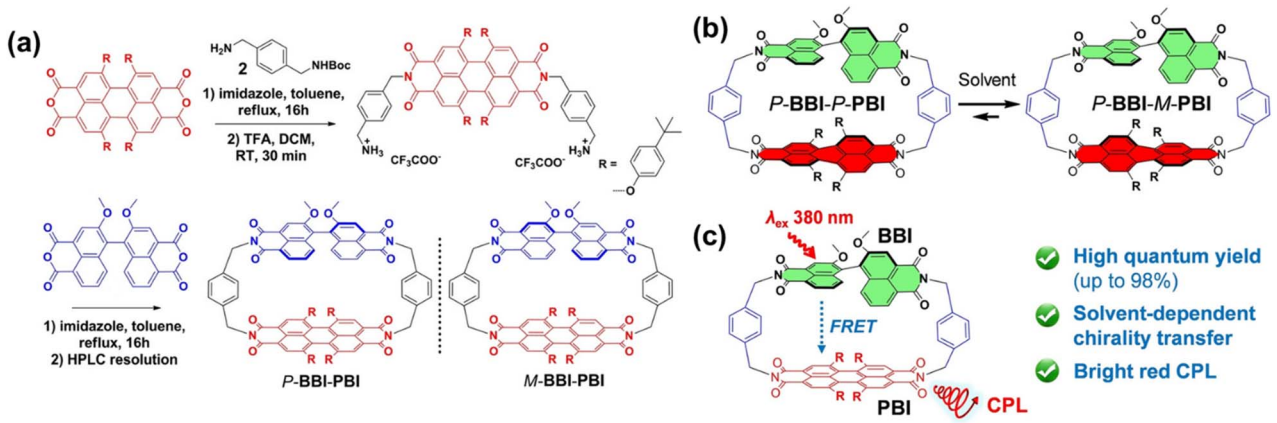

Fig. 5 (a) Synthesis of **BBI-PBI**; schematic illustration of (b) the chiral transfer and (c) the energy transfer processes in **BBI-PBI**. Reproduced from ref. 64. Copyright 2022 Wiley-VCH.

design strategy for heterochiral molecular receptors based on steric hindrance modulation.

Beyond utilizing host–guest interactions, the incorporation of PBI alongside other chiral units into the cyclophane backbone provides an alternative strategy for harnessing the chirality and optical properties of PBI. The research group successfully constructed a chiral luminescent cyclophane, **BBI-PBI**, comprising a chiral binaphthol bisimide (BBI) unit and a conformationally labile, bay-substituted PBI unit (Fig. 5a and b).[64] This molecule exhibits distinctive intramolecular energy transfer and solvent-modulated chiral transfer, whereby energy is channeled from the BBI unit to the PBI unit. Additionally, owing to the ideal spectral overlap and spatial alignment between the donor BBI and the acceptor PBI, the system enables quantitative Förster resonance energy transfer (FRET). Upon excitation of the BBI unit, the PBI unit generates highly efficient CPL with amplified CPL signals (Fig. 5c). Through the elegant integration of both energy transfer and chiral transfer within a single molecule, this work showcases the considerable potential of PBI-based cyclophanes as versatile platforms for multi-channel information processing and sensing applications.

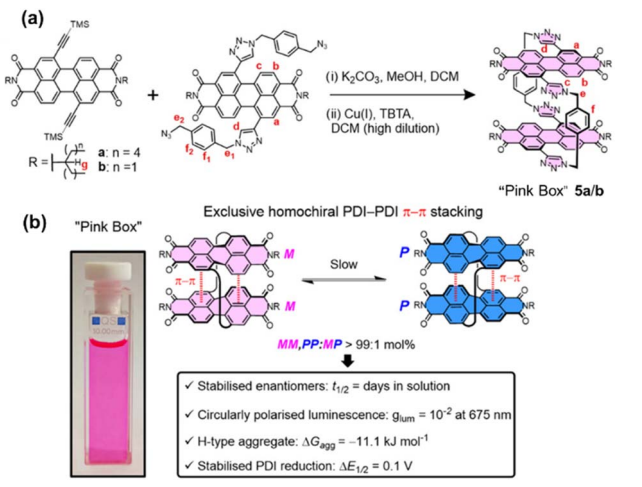

Fig. 6 (a) Synthesis of the "Pink Box" **5a/b** *via* CuAAC reaction; (b) schematic illustration of the distinctive homochiral π–π stacking within the Pink Box. Reproduced from ref. 66. Copyright 2022 American Chemical Society.

The bay positions of PBI units can also be utilized to link other components for constructing cyclophanes.[65] The team of Barendt has conducted systematic research on such cyclophanes in recent years, achieving breakthrough results. They constructed the first cyclophanes **5a/b** of this type, termed the "Pink Box", featuring two PBI units, *via* copper(I)-catalyzed azide–alkyne cycloaddition (CuAAC) click chemistry (Fig. 6a).[66] This molecule undergoes highly specific homochiral stacking in toluene. The strong intramolecular π–π interactions within this homochiral arrangement greatly stabilize its configuration, extending the enantiomer half-life by more than 400-fold (from minutes to days). Notably, the structure possesses CPL with an exceptionally high luminescence dissymmetry factor ($|g_{lum}| = 10^{-2}$) and outstanding electron-accepting capability (Fig. 6b), underscoring the great promise of utilizing cyclophane design to realize homochiral stacking for enhancing chiroptical and electrochemical properties. They also developed a novel strategy employing supramolecular interactions to guide the stereoselective synthesis of chiral macrocycles. They pioneered the application of the Curtin–Hammett principle to macrocyclization reactions, designing a cyclophane **6** which composed of a dynamically racemic PBI unit and a configurationally stable *P*-BINOL (Fig. 7a).[67] Surprisingly, the reaction preferentially produced the heterochiral isomer (*PM*) with notable selectivity (d*r* = 4 : 1), contrary to computational predictions based on thermodynamic stability of the products (Fig. 7b). The origin of this selectivity lies in the lower transition state energy for the formation of the heterochiral macrocycle, leading to the highly selective synthesis under kinetic control. This research paves a new pathway for preparing chiral macrocyclic compounds that are not thermodynamically favored.

Previous work has separately explored the feasibility and unique properties of constructing chiral cyclophanes by utilizing either the imide or the bay positions of PBI as

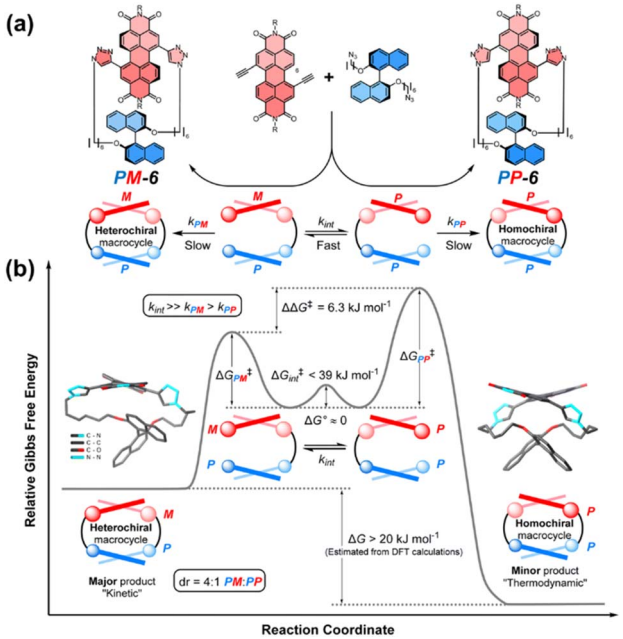

Fig. 7 (a) Schematic structure of cyclophanes *PP*/*PM*-6; (b) energy profile diagram for the diastereoselective synthesis of macrocycle *PM*-6 under Curtin–Hammett control. Reproduced from ref. 67. Copyright 2024 Royal Society of Chemistry.

connection points. The Würthner group integrated these two strategies, developing a PBI cyclophane system that employs simultaneous and synergistic connection at both the bay and imide positions. Specifically, they first constructed a stable, inherently chiral PBI building block *via* intramolecular bridging at the bay positions, followed by macrocyclization through the imide positions, thereby facilitating control over its size and cavity dimensions. Based on this approach, they pioneered the synthesis of the inherently chiral PBI cyclophanes 7-***MM*** and 7-***PP*** (Fig. 8a).[68] The cavity of this cyclophane exhibited extremely high affinity for homochiral helicenes, with a binding constant for [4]-helicene as high as 3.9×10^{10} M^{-1}, and it successfully functioned as a template for the deracemization of [5]-helicene, achieving an enantiomeric excess (e.e.) value of 66% (Fig. 8b and c). Using 7-***PP*** as an example, mechanistic studies revealed that the cyclophane stabilizes the reaction transition state through π–π interactions, accelerating the enantiomerization rate by approximately 700-fold.[69] In contrast, the meso-isomer 7-***MP*** showed no such catalytic activity, highlighting the crucial role of precise matching between the chiral cavity and the transition state structure in achieving π–π catalysis (Fig. 8d). Subsequently, by extending the linker at the imide position, they constructed larger-cavity PBI cyclophanes, **cyc-*PP*/cyc-*MM*** (Fig. 9a).[70] This macrocycle can cooperatively bind two aromatic guests (*e.g.*, coronene) with a remarkably high cooperativity factor of 485 (Fig. 9b). Furthermore, this system accomplished the transfer of host chirality to the achiral guest and, for the first time in a solution-phase non-covalent host–guest system, observed CPL originating from a charge-transfer state (CT-CPL), with the $|g_{lum}|$ value increased to 2×10^{-3} (Fig. 9c). This series of works demonstrates that by synergistically utilizing both the bay and imide positions of PBI, it is possible to systematically

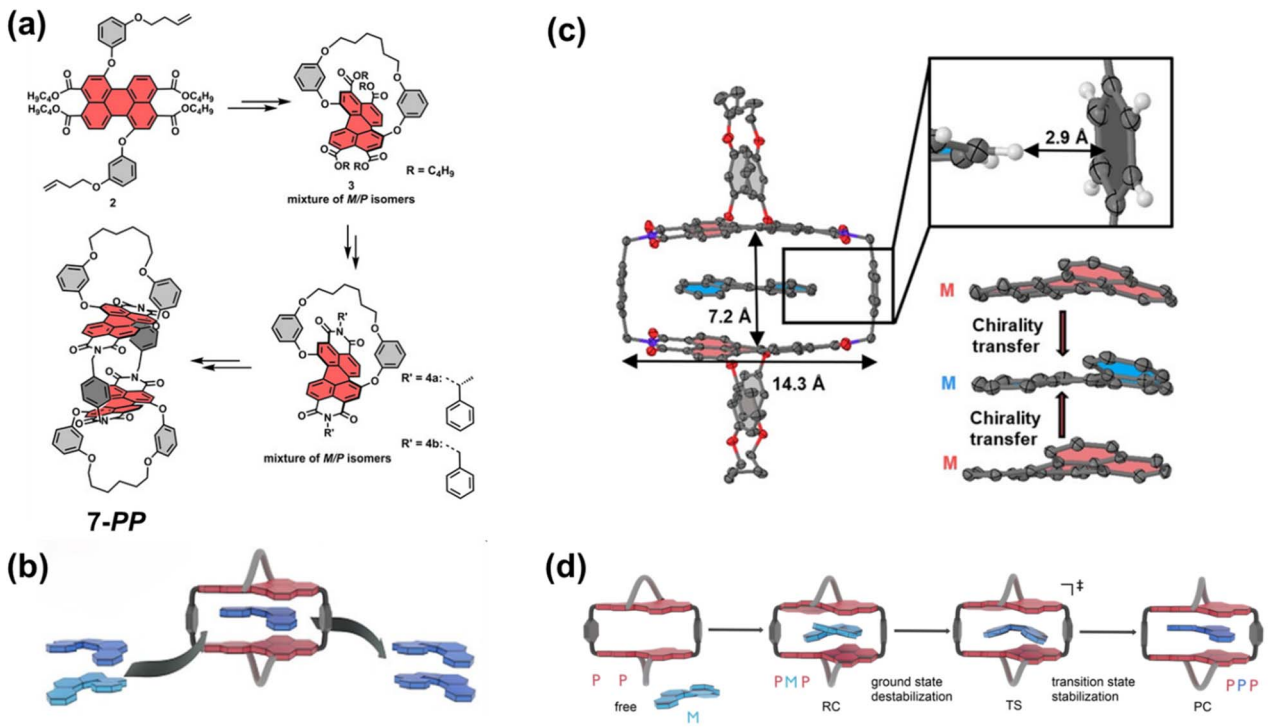

Fig. 8 (a) Synthesis of cyclophanes 7-*PP*; (b) process of [5]helicene deracemization within 7-*PP*; (c) single-crystal structure of the *M*-[4]helicene⊂7-*MM* complex; Reproduced from ref. 68. Copyright 2021 Wiley-VCH. (d) Proposed mechanism for the enantiomerization of [5]helicene within 7-*PP*. Reproduced from ref. 69. Copyright 2023 Wiley-VCH.

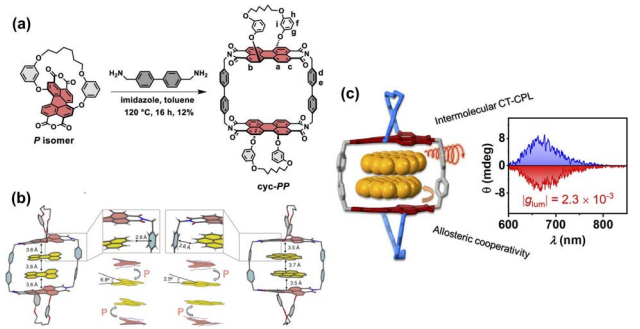

Fig. 9 (a) Synthesis of cyclophane **cyc-*PP***; (b) single-crystal structures of (perylene)$_2$⊂**cyc-*PP*** (left) and (coronene)$_2$⊂**cyc-*PP*** (right); (c) schematic illustration of the intramolecular CT-CPL in the host–guest complexes. Reproduced from ref. 70. Copyright 2024, American Chemical Society.

tune the cavity size and chiral microenvironment of the cyclophanes. This approach has successfully enabled the realization of a range of complex functions, from highly efficient chiral recognition and asymmetric catalysis to the modulation of multivariate cooperative photophysical properties.

In addition to the aforementioned axially chiral aromatic units, helicenes with their inherent helical chirality serve as ideal platforms for constructing functionalized chiral cyclophanes. Chen *et al.* has achieved a series of important advances in this field in recent years. They utilized configurationally stable [5]helicenes as chiral sources and successfully constructed a series of B/N-doped chiral cyclophanes (**CMC1**, **CMC2**, **CMC3**) by introducing triarylborane/amine groups (Fig. 10a).[71] These compounds exhibit unique photoelectronic properties, with the CPL response of **CMC3** extending into the near-infrared region (Fig. 10b). Building on this, they further developed an electron-rich chiral cyclophane **8** based on aza[7]helicene as the core building block (Fig. 11).[72] This molecule also shows superb luminescent properties and high brightness

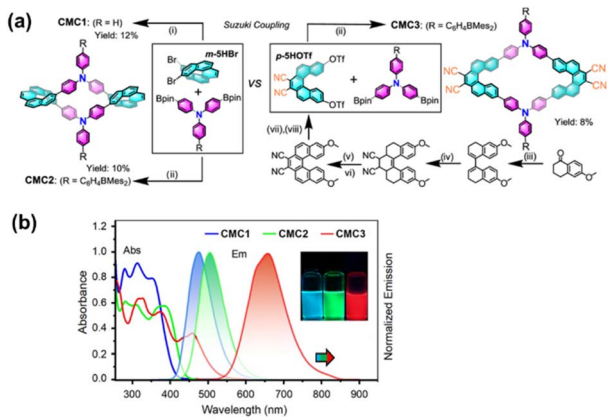

Fig. 10 (a) Synthesis of [5]helicene-based B/N-doped main-group chiral macrocycles **CMC1**, **CMC2**, and **CMC3**; (b) absorption and emission spectra of **CMC1**, **CMC2**, and **CMC3** ($\lambda_{ex} = \lambda_{abs(max)}$, $c = 1.0 \times 10^{-5}$ M) in CH_2Cl_2. Inset: emission photographs under 365 nm UV irradiation. Reproduced from ref. 71. Copyright 2023, American Chemical Society.

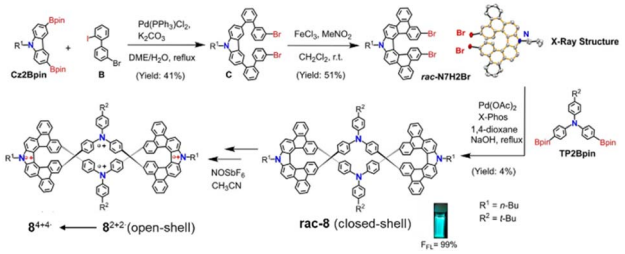

Fig. 11 Synthesis of **8** and the formation of polyradical cationic cyclophanes by redox chemistry. Inset: photographs of emission in CH_2Cl_2 under 365 nm UV light. Reproduced from ref. 72. Copyright 2024 Wiley-VCH.

of CPL (B_{CPL}). More significantly, it can undergo stepwise and controllable chemical or electrochemical oxidation to generate a series of multicationic open-shell species whose electronic states depend on the oxidation level. This research underscores the application value of such systems in fields like chiral spintronics and superconductors.

2.2 Cyclophanes with chirality from the linkers

In contrast to π-system-centered chirality, another important design strategy involves introducing chirality through linker units that connect aromatic frameworks within cyclophane architectures. These linkers may consist of aliphatic chains, heteroatom-containing bridges, or axially chiral aromatic building blocks such as BINOL and biphenyl derivatives. In such systems, the chiral unit primarily acts as a structural bridge or conformational regulator, while the principal π-system of the macrocycle remains achiral or only secondarily influenced by the axial element. Consequently, the overall chirality of the cyclophane is derived from the linker rather than the intrinsic π-framework.

Naturally occurring chiral molecules represent an important source of chirality. Among them, amino acids, owing to their diverse types and ease of derivatization, are frequently employed as chiral linkers in cyclophane construction. For instance, they can be incorporated through various modifications into imidazolium-based cyclophanes and tetraazacyclophanes, thereby endowing the molecules with biocompatibility.[73–75] Recently, Xing and coworkers reported a class of heteroatomic chiral cyclophanes **9a** and **9b** whose chirality originates from L- or D-leucine/phenylalanine groups connected *via* amide bonds (Fig. 12a).[76] In aqueous solution, these chiral cyclophanes can undergo self-assembly driven by anion-recognition effects, successfully transferring and amplifying the central chirality of the amino acids into supramolecular chirality. Upon introduction of surface-positively charged amino nanoclay (AC), the electrostatic interactions between the cyclophanes and the clay disrupt the initial anion recognition. This leads to a reconfiguration of the supramolecular assembly and results in an inversion of the CD signal, achieving switchable supramolecular chirality (Fig. 12b).

Likewise, carbohydrates, which are readily available and easily modifiable natural chiral sources, have also been

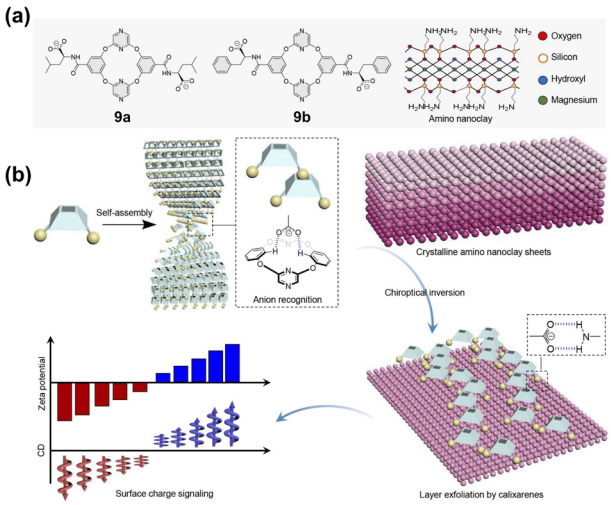

Fig. 12 (a) Structures of **9a**, **9b**, and AC; (b) schematic illustration of the self-assembly and co-assembly of **9a**. Reproduced from ref. 76. Copyright 2024 American Chemical Society.

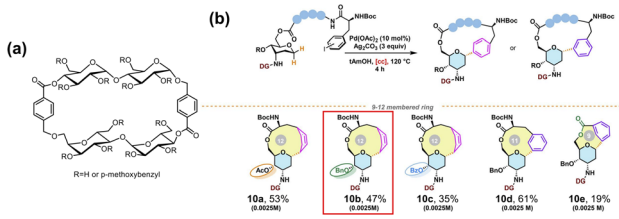

Fig. 13 (a) Representative structure of a glycophane; (b) palladium-catalyzed enantioselective synthesis of small-sized glycophanes **10a–e** with high ring strain. Reproduced from ref. 84. Copyright 2024 Wiley-VCH.

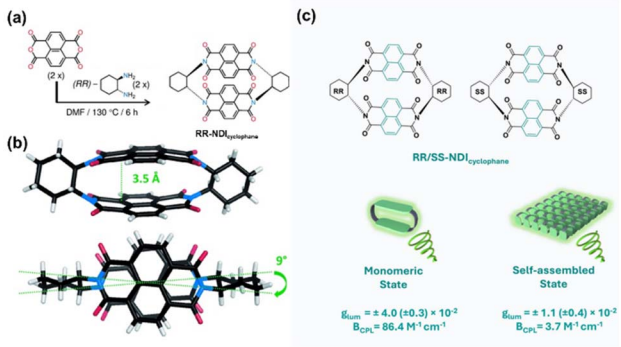

Fig. 14 (a) Synthesis of RR-NDI$_{cyclophane}$; (b) solid-state structure of RR-NDI$_{cyclophane}$ in both top and side views; Reproduced from ref. 85. Copyright 2014 WILEY-VCH. (c) Schematic representation of key CPL parameters, including g_{lum} and B_{CPL}, for the monomeric and self-assembled states of ***RR*/*SS*-NDI$_{cyclophane}$**. Reproduced from ref. 86. Copyright 2025 WILEY-VCH.

employed in the construction of cyclophanes. The resulting hybrids of carbohydrates and cyclophanes are termed glycophanes (Fig. 13a) and exhibit high application potential in chemical biology.[77–83] Recently, Bazzi and colleagues reported a novel strategy for constructing glycophanes *via* palladium-catalyzed enantioselective C(sp^3)-H cyclization, leading to the successful synthesis of a series of novel small-sized glycophanes with high ring strain (Fig. 13b).[84] Biological evaluation revealed that glycophane **10b** exhibits marked anti-proliferative activity against human colon cancer cells HCT-116. This work not only broadens the synthetic approaches for glycophanes but also establishes their utility as a chiral molecular platform with biological activity in chemical biology.

Stoddart and colleagues developed a cyclophane system (Fig. 14a and b), ***RR*/*SS*-NDI$_{cyclophane}$**, based on (*RR*)- or (*SS*)-*trans*-1,2-diaminocyclohexane and naphthalene diimide (NDI).[85] This system constructs a rigidly co-facially stacked NDI dimeric cyclophane, revealing its unique exciton coupling, long-lived excimer emission, and rich redox behavior. Recently, the George team successfully evolved this system into a highly efficient, color-tunable CPL material (Fig. 14c).[86] These **NDI$_{cyclophane}$** molecule exhibit highly efficient intramolecular excimer emission even in its monomeric state, combining high B_{CPL} and high quantum yield, and represents one of the brightest green CPL emitters reported to date. It achieves a luminescence dissymmetry factor as high as 4.0×10^{-2} and a B_{CPL} of 86.4 M^{-1} cm^{-1}. This work vividly demonstrates that through the ingenious use of linker chirality, macrocyclic systems with specific supramolecular interactions and outstanding chiroptical functions can be purposefully constructed.

Beyond their inherent chirality, chiral linkers can also precisely control the higher-order topological structure of macrocyclic hosts, such as their overall helical chirality, through their spatial configuration. Haino and coworkers reported a chiral twisted tetraphenylporphyrin cyclophane **(*R*,*R*)/(*S*,*S*)-11** constructed by incorporating chiral dioxolane-based linkers (Fig. 15b).[87] This molecule exhibits unique solvent-dependent conformational preferences: it primarily adopts an (*M*)-helical conformation in nonpolar aromatic solvents (*e.g.*, toluene), while stabilizing in a (*P*)-helical conformation in polar solvents such as DMF, halogenated solvents (*e.g.*, CH_2Cl_2), and polar aromatic solvents (*e.g.*, benzonitrile). Analysis by CD spectroscopy and theoretical calculations confirmed that both solvent polarity and molecular structure cooperatively regulate the relative stability of different chiral conformations, leading to inversion of the helical sense in different solvent environments. This study reveals the solvent-responsive nature of chiral porphyrin cyclophanes, provides new insights into understanding their structural dynamics, and expands their application prospects in areas such as chiral detection and sensing.

In addition to traditional carbon-centered chirality, the asymmetric coordination environment of metal centers can also serve as an origin of chirality in cyclophanes, opening new pathways for constructing chiral cyclophane systems with unique structures and properties. Yip and coworkers elucidated a tetranuclear gold(I) cyclophane structure **12** whose chirality originates from two non-carbon chiral centers in the molecule: a sulfonium ion and a gold(I) ion (Fig. 16a).[88] In each Au_2S_2 unit, one sulfur atom bonds to two gold ions with distinct chemical

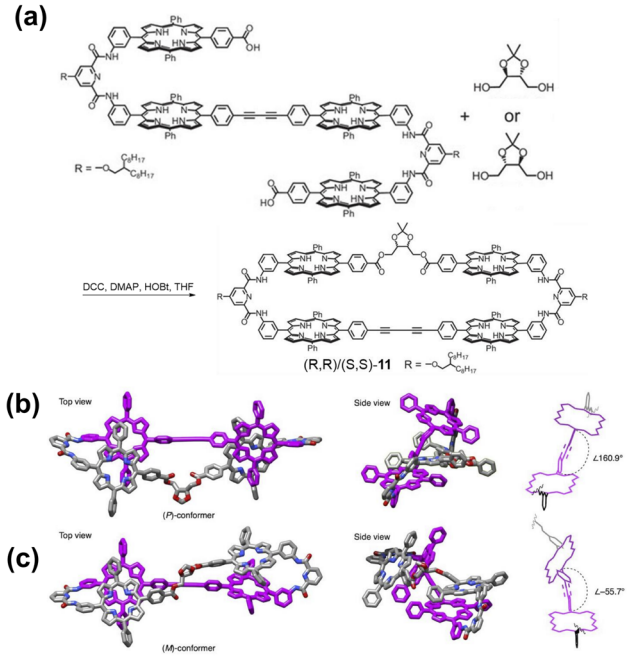

Fig. 15 (a) Synthesis of the chiral twisted tetraphenylporphyrin cyclophane enantiomers (*R*,*R*)/(*S*,*S*)-**11**; computationally optimized geometries of (*R*,*R*)-**11** in the (b) (*P*)- and (c) (*M*)-conformations. Reproduced from ref. 87. Copyright 2025 WILEY-VCH.

environments, constituting a chiral sulfur center; simultaneously, one gold(I) ion resides in an asymmetric environment composed of four coordinating atoms—S(1), S(2), P, and Au—resulting in a rare gold(I)-centered chirality. X-ray crystallography revealed that the two Au_2S_2 cores of the cyclophane adopt R_{Au},R_S and S_{Au},S_S configurations, respectively. Variable temperature NMR studies revealed that this cyclophane undergoes rapid dynamic exchange in solution through intramolecular concerted Au–S bond cleavage and formation, yet this process does not alter the inherent chiral configuration of each chiral center (Fig. 16b). This work not only realizes gold-centered chirality in a cyclophane for the first time, but also illustrates how the dynamic nature of metal–ligand coordination bonds can confer molecules with conformationally dynamic behavior.

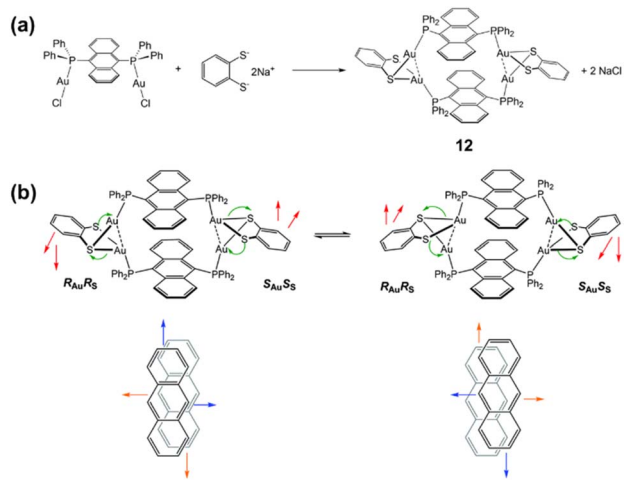

Fig. 16 (a) Structure of the tetranuclear gold(I) cyclophane **12**; (b) schematic representation of the intramolecular dynamic exchange of Au–S bonds. Reproduced from ref. 88. Copyright 2021 Royal Society of Chemistry.

Among axially chiral linkers, allenes serve as an ideal platform for constructing structurally unique cyclophanes known as allenophanes, owing to their inherent axial chirality and conformational rigidity. These molecules can function as electron-rich, sterically demanding chiral ligands or as hosts for metal ions and small molecules, holding significant value for investigating structure-chiroptical property relationships.[89] Following early, less systematic studies,[90,91] Thorand and colleagues achieved the synthesis of the first well-defined allenophane.[92] However, the synthetic route lacked stereoselectivity and afforded low overall yield. Subsequent studies introduced the Sharpless asymmetric epoxidation to achieve stereospecific synthesis of the isomers[93,94] or employed high-performance liquid chromatography for chiral separation,[95,96] thereby addressing the challenge of obtaining single-isomer allenophanes.

In recent years, Cid's team has obtained a series of breakthroughs in the preparation and functionality of new allenophanes. They first reported a chiral bipyridoallenophane (***P*,*P***)-**13** with a single conformation and strong chiroptical response, exhibiting a high *g* factor of 0.007 (Fig. 17a).[97] (***P*,*P***)-**13** undergoes an unusual double protonation process in non-aqueous solvents, driven by cooperative ion-pairing and hydrogen-bonding interactions within its bipyridine units (Fig. 17b). This process forces the bipyridine axis into a single configuration and generates a characteristic CD signal at 330 nm. In their subsequent work, they efficiently prepared a novel pyridoallenophane **14** (Fig. 17c).[98] Through CD spectroscopy and Brønsted correlation analysis, it was found that complete proton transfer to the pyridine occurs regardless of the acid's pK_a, forming a doubly protonated species accompanied by counterion coordination (Fig. 17d). This series of studies paves the way for designing and customizing novel synthetic receptors: by precisely controlling the spatial arrangement of pyridine groups in allenophanes, high-selectivity, high-affinity recognition of specific anions or ion pairs can be established, demonstrating the great potential of this class of cyclophanes in the field of tailored synthetic receptors.

Beyond aliphatic and allene-type linkers, axial chirality embedded within aromatic linker units also represents an important strategy for constructing chiral cyclophanes. In these systems, axially chiral motifs such as BINOL or biphenyl derivatives serve primarily as structural bridges between larger π-frameworks. Although these aromatic units themselves are π-conjugated, their role in the macrocycle is fundamentally different from that of a chiral π-core; instead, they function as configurationally stable chiral connectors that impose stereochemical bias on the overall framework.

For instance, Cao and coworkers prepared a pair of water-soluble tetraimidazolium cyclophane (Fig. 18a) ***RR*/*SS*-15**·4Cl^-

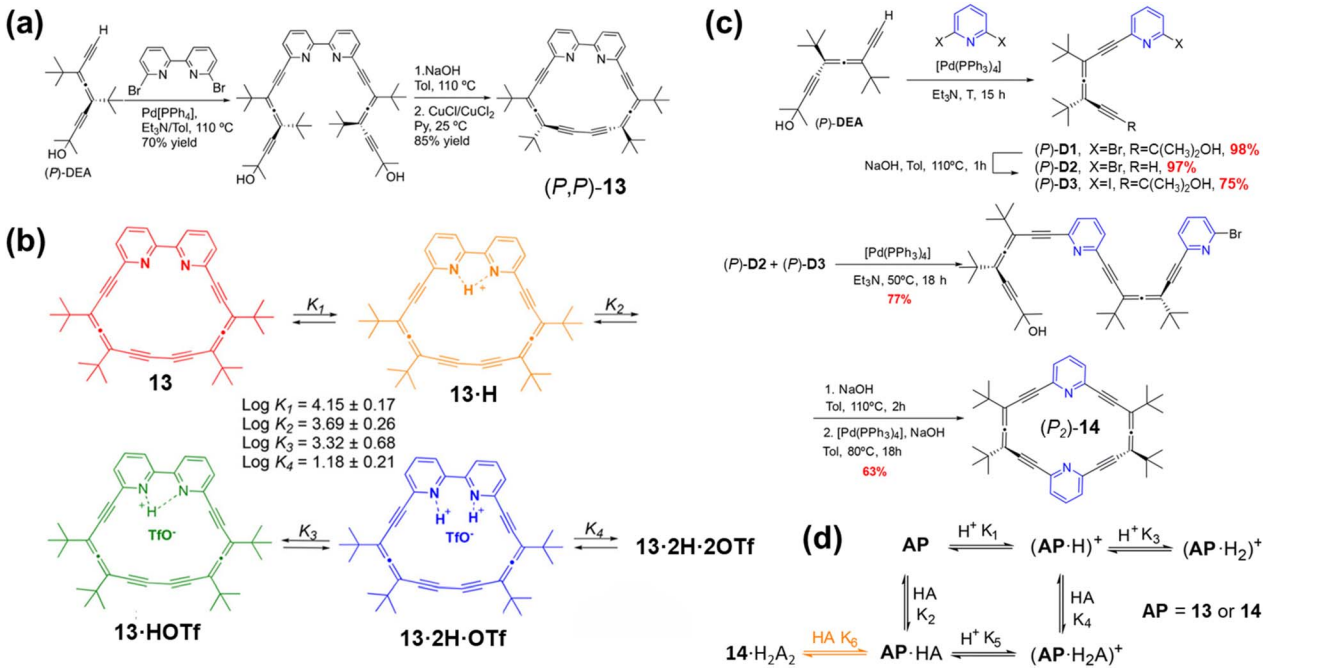

Fig. 17 (a) Synthesis of allenophanes **13**; (b) proposed scheme for titration process for (*P,P*)-**13** with TfOH in CH_3CN; Reproduced from ref. 97. Copyright 2019, American Chemical Society. (c) Synthesis of allenophanes **14**; (d) titration scheme for allenophanes **13** and **14** with oxoacids. The equilibrium in orange is only relevant for compound **14**. (AP = Allenophane). Reproduced from ref. 98. Copyright 2023, Royal Society of Chemistry.

which exhibits temperature-dependent conformational behavior.[99] As the temperature increases, its conformation can switch from *cis* to *trans*, thereby transforming the cavity from a closed to an open state (Fig. 18b). This property substantially enhances its binding constant for the dinucleotide d(TpA) from approximately 10^4 M^{-1} at 288 K to about 10^6 M^{-1} at 323 K, while its affinity for other dinucleotides (d(ApT), d(GpC), and d(CpG)) decreases with increasing temperature. As a result, high selectivity for the complementary dinucleotide pair d(TpA)/d(ApT) was attained, with the selectivity factor (K_{rel}) increasing markedly from 1.1 to 118.8 (Fig. 18c). This work powerfully exemplifies how the conformational dynamics of BINOL-based cyclophanes can be harnessed through molecular design to realize tunable molecular recognition.

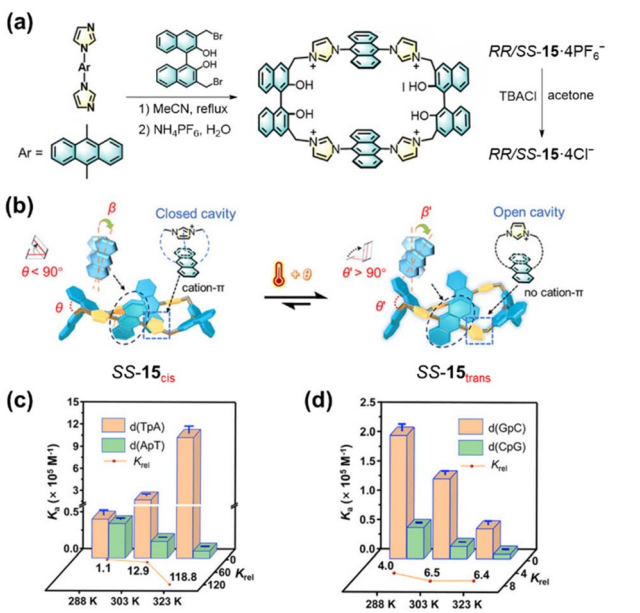

Fig. 18 (a) Synthesis of *RR*/*SS*-**15**·$4Cl^-$; (b) mechanism of the conformational change of *SS*-**15**; comparison of the binding constants (K_a) and K_{rel} of *SS*-**15**·$4Cl^-$ with (c) d(TpA)/d(ApT) and (d) d(GpC)/d(CpG). Reproduced from ref. 99. Copyright 2025 Wiley-VCH.

Along this line, Hasegawa and co-workers reported stereogenic macrocycles composed of axially chiral binaphthyl units bridged by bithiophene linkers, affording cyclic dimers [2]-**16** and trimers [3]-**16** *via* Ni(0)-mediated homocoupling (Fig. 19).[100] The binaphthyl moieties serve as configurationally stable axial chiral linkers, while the orientation of the bithiophene bridges (*s-cis versus* s-*trans*) significantly modulates the overall macrocyclic geometry. Notably, the cyclic dimer exhibited a rare bisignate-type CPL spectrum, with sign inversion within a single emission profile, arising from the coexistence of energetically comparable conformers possessing opposite rotatory strengths. In contrast, the cyclic trimer displayed a more regular CPL response, consistent with its reduced strain and less restricted conformational behavior.

Ordinary biphenyl molecules are typically achiral due to free rotation around the carbon–carbon single bond connecting their two benzene rings. However, when sufficiently bulky substituents are introduced at the ortho positions to restrict this bond rotation, the biphenyl unit can transform into stable

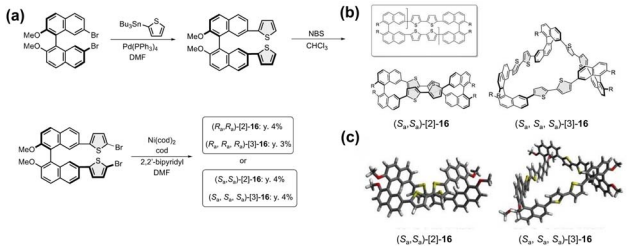

Fig. 19 (a) Synthetic route, (b) molecular structure, and (c) optimized structure of [*n*]-X (*n* = 2 and 3). Reproduced from ref. 100. Copyright 2025 Wiley-VCH.

atropisomers, thereby exhibiting axial chirality. Early research work employed the conformational properties of biphenyl units to construct double-helical topological structures and explored their possible applications as chiral sensors.[101,102] In recent years, the research focus has shifted more toward achieving highly enantioselective synthesis of cyclophanes and further expanding their functions in areas such as chiral recognition. To address the synthetic challenge of precise control over axial chirality, Speicher's team devised a chiral sulfinyl group-assisted enantioselective Heck coupling/macrocyclization strategy and successfully applied it to the total synthesis of various cyclophane-type natural products.[103,104] They first detailed the enantioselective total synthesis of Isoplagiochin *D* (Fig. 20a), where this strategy enabled efficient control over the stereochemistry of the biphenyl axis while constructing the cyclophane skeleton, ultimately affording the target molecule with 98% ee. Subsequently, the team refined this approach by adopting a more atom-economical C–H activation Heck-type coupling reaction to produce Isoriccardin C (Fig. 20b), achieving similarly excellent enantioselectivity (ee >98%). This series of studies accomplished the first *atropo*-diastereoselective total synthesis of such natural products, providing a new strategy for precise chiral control in this class of cyclophanes.

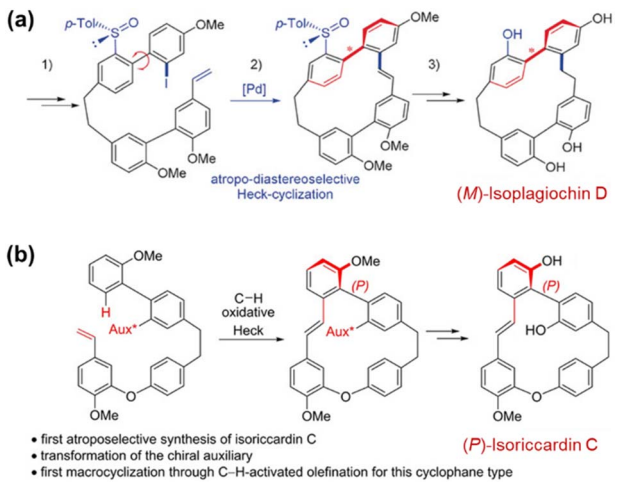

Fig. 20 Atropo-diastereoselective Heck coupling for the synthesis of enantiopure (a) Isoplagiochin D Reproduced from ref. 103. Copyright 2018 Wiley-VCH and (b) Isoriccardin C. Reproduced from ref. 104. Copyright 2021 Wiley-VCH.

Beyond these representative BINOL- and biphenyl-based systems, other sterically congested aromatic frameworks have also been developed as axially chiral linker motifs. Itami and co-workers introduced 4,5-diphenylphenanthrene as a novel axially chiral three-dimensional building block for the construction of highly twisted macrocycles **17** *via* quadruple Suzuki–Miyaura coupling (Fig. 21a and b).[105] The steric congestion at the 4,5-positions enforces a pronounced helical distortion, and single-crystal X-ray analysis revealed that the resulting macrocycles adopt nearly perpendicular π-arrangements with twist angles approaching 90° (Fig. 21c). Notably, macrocyclization significantly enhances configurational stability: whereas the monomeric building block displays a moderate helical inversion barrier, the corresponding macrocycle exhibits a racemization barrier of approximately 31 kcal mol^{-1}, as confirmed by both DFT calculations and kinetic measurements. Furthermore, the C_2-symmetric alignment of two axially chiral subunits leads to amplified circular dichroism responses compared to the monomeric counterpart. Collectively, these examples illustrate that aromatic axial chiral linkers not only provide robust stereochemical elements for macrocyclization, but also enable fine regulation of cavity geometry, stereochemical stability, and chiroptical behavior through structural constraint.

2.3 Cyclophanes with planar chirality

Distinct from the types of chirality dominated by specific chiral units discussed above, planar chirality represents a unique form of asymmetry. It does not originate from a traditional chiral center or axis, but arises because the macrocyclic structure

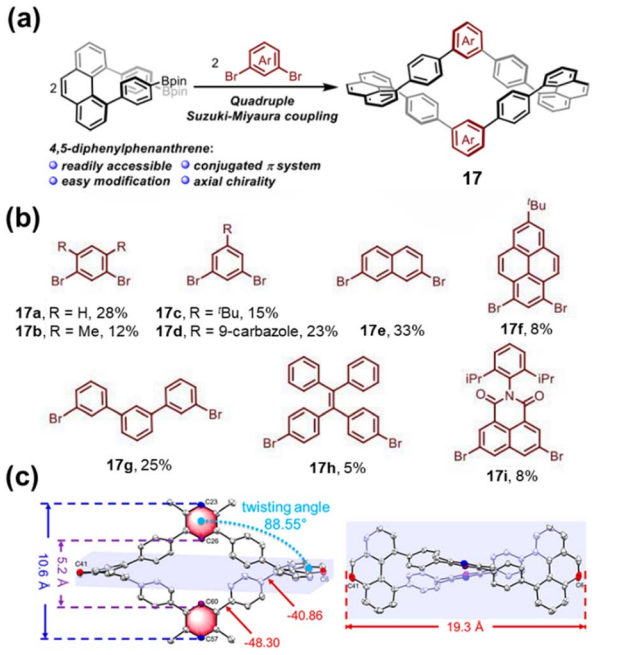

Fig. 21 (a) The synthesis of the highly twisted macrocycle **17** from the 4,5-diphenylphenan-threne core; (b) yields of Xa–i and the structures of the corresponding aryldibromide reactants; (c) X-ray structure of **17b** at 50% thermal probability. Reproduced from ref. 105. Copyright 2020 American Chemical Society.

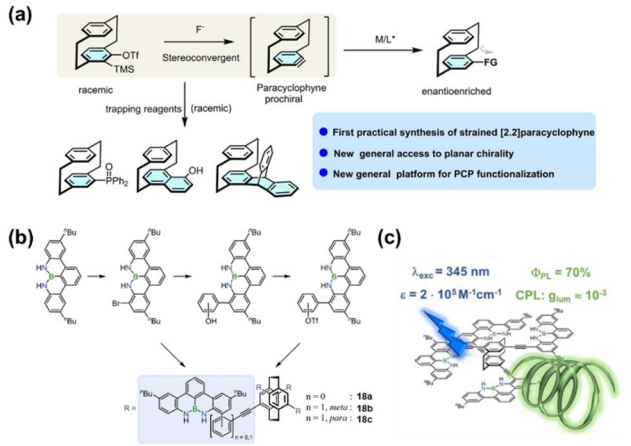

Fig. 22 (a) Formation of the aryne analogue intermediate and its subsequent transformations; Reproduced from ref. 109. Copyright 2025 Wiley-VCH. (b) Synthesis of novel BN-doped planar chiral [2.2] paracyclophane derivatives **18a–c**; (c) luminescence properties of **18a**, including high quantum yield and CPL activity. Reproduced from ref. 110. Copyright 2021 Wiley-VCH.

prevents the free flipping of aromatic planes, thereby conferring asymmetry. Among these, the most typical representative is PCP and its derivatives. PCP consists of two face-to-face stacked benzene rings connected by two ethyl chains.[14,15] The benzene rings cannot undergo free rotation around the bonds linking them to the bridges. When the substitution patterns on the two benzene rings are asymmetric, the molecule loses its symmetry plane, resulting in planar chirality. Beyond its unique structure, PCP also exhibits unique electronic and photophysical properties, making this molecule an ideal platform for exploring phenomena and functions related to planar chirality.

Building upon the PCP scaffold, researchers have constructed structurally diverse derivatives through regioselective synthesis and efficient functional group transformations to achieve distinct substitution patterns. Enantiopure compounds have been obtained *via* chiral resolution techniques. These breakthroughs in synthetic strategies have laid the foundation for exploring their applications in asymmetric catalysis, chiral ligand design, and CPL materials.[106–108]

Recent research has focused primarily on two aspects. The first involves developing synthetic strategies for novel PCP derivatives. For example, Xu and coworkers pioneered a synthetic strategy based on a dehydrogenated PCP intermediate. Using asymmetric copper(I) catalysis, they efficiently accomplished enantioconvergent alkynylation of this *in situ* generated intermediate with excellent enantioselectivity (Fig. 22a).[109] This key intermediate can participate in various aromatic nucleophilic substitution and cycloaddition reactions, facilitating the preparation of diverse functionalized PCPs. The second aspect focuses on integrating functional units with the PCP scaffold to enable sophisticated functions and applications. For instance, Bettinger and colleagues introduced BN-doped polycyclic aromatic hydrocarbon (PAH) units into a multisubstituted PCP for the first time, yielding novel PCP derivatives **18a–c** (Fig. 22b).[110] These compounds exhibit excellent optical and chiroptical properties, with a fluorescence quantum yield of 0.70 for **18a** and notable CPL activity (Fig. 22c). This BN-doping approach opens a new avenue for developing high-performance CPL materials. In a separate study, Bräse and coworkers reported a breakthrough in planar chiral thermally activated delayed fluorescence (TADF) materials. They synthesized the first such emitter (1,4)*t*BuCzpPhTrz(**19**) based on a rearranged PCP-derived skeleton, which was accessed through a novel intramolecular rearrangement reaction. This structural modification successfully realized a breakthrough in TADF performance, providing a unique approach for designing chiral TADF systems (Fig. 23).[111]

Beyond the aforementioned work, PCP possesses distinct advantages in constructing functional molecules with chiral topological structures. This research generally follows a core

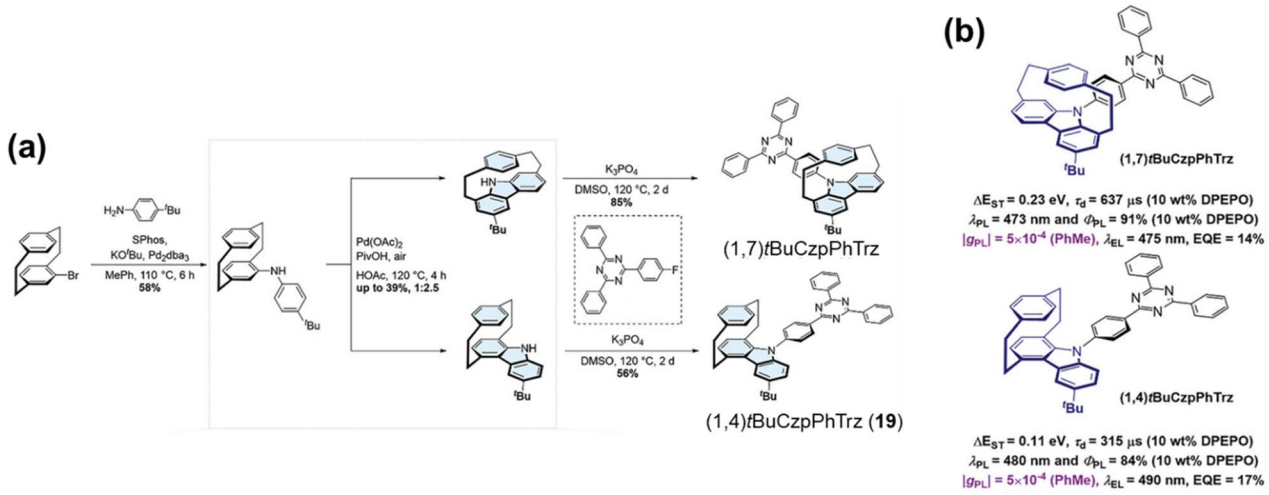

Fig. 23 (a) Synthesis and (b) optical properties of (1,4)tBuCzpPhTrz (**19**) and its regioisomer (1,7)tBuCzpPhTrz. Reproduced from ref. 111. Copyright 2024 Wiley-VCH.

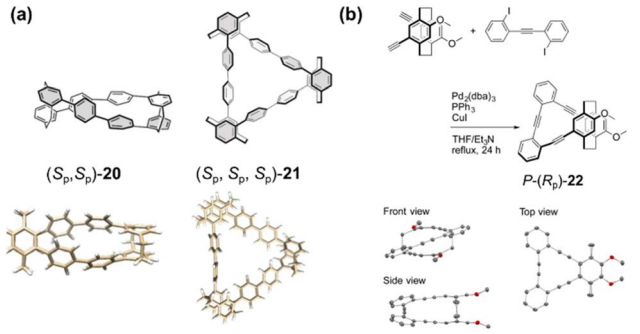

Fig. 24 (a) Molecular structures (top) and computed optimized structures (bottom) of dimer (S_p,S_p)-**20** and trimer (S_p,S_p,S_p)-**21**; Reproduced from ref. 116. Copyright 2021 Wiley-VCH. (b) Synthesis (top) and molecular structure (bottom) of *P*-(R_p)-**22**. Reproduced from ref. 117. Copyright 2022 The Chemical Society of Japan.

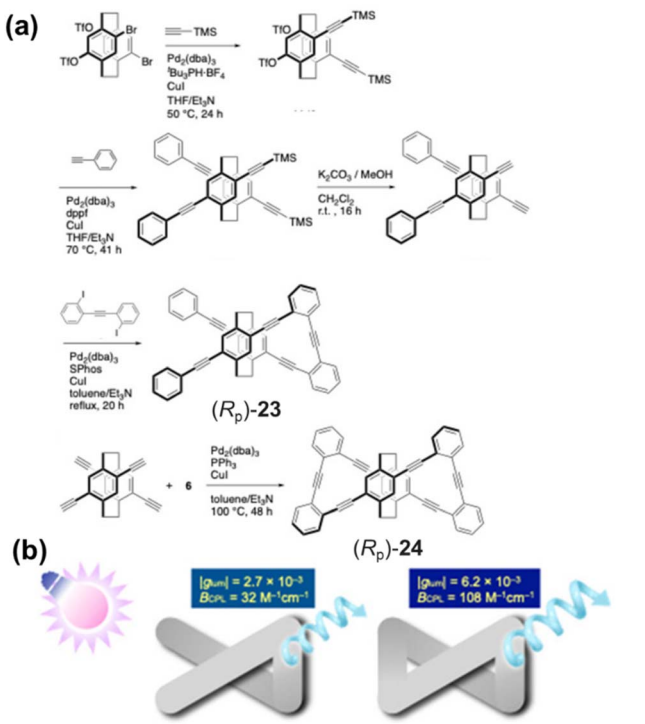

Fig. 25 (a) Synthesis and (b) CPL properties of (R_p)-**23** and (R_p)-**24**. Reproduced from ref. 118. Copyright 2025 Wiley-VCH.

strategy: using PCP as a chiral source and transmitting its chiral information into larger π-conjugated frameworks through covalent linkages, thereby constructing advanced architectures with remarkable optical activity.[112–115]

Based on this strategy, Hasegawa and coworkers successfully constructed dimer **20** and trimer **21** connecting PCP with biphenyl units (Fig. 24a).[116] The dimer adopts a double-helical structure, while the trimer forms a chiral triangular topology. Both compounds exhibit strong optical activity, featuring high fluorescence quantum yields and $|g_{lum}|$ value on the order of 10^{-3}. This work showcases the capability of utilizing the planar chirality of PCP to construct three-dimensional topological structures and produce high-performance chiral optical dyes. Building on this foundation, the team of Morisaki synthesized a pair of enantiopure single-handed helical molecules (***P*-(R_p)-** and ***M*-(S_p)-22**) based on PCP, whose helical chirality is precisely governed by their planar chirality (Fig. 24b).[117] This system exhibits exceptional chiroptical properties, with a $|g_{lum}|$ value as high as 10^{-2}. Combined experimental and theoretical studies confirmed that the key to achieving such high $|g_{lum}|$ lies in the formation of a unified π-conjugated system with optimal arene overlap enforced by the PCP scaffold. Furthermore, by extending the π-conjugated system, they successfully constructed ribbon-like and propeller-shaped three-dimensional architectures (**23** and **24**).[118] The propeller-shaped molecule, with its more extensive conjugation, displays superior characteristics including high $|g_{lum}|$ and high B_{CPL} (Fig. 25). This series of studies convincingly demonstrates that employing PCP as a photoactive core enables the construction of diverse optically active stereochemical topologies and provides an unambiguous molecular-level design blueprint for developing high-performance CPL-emitting materials.

Indeed, planar chirality can potentially arise in any cyclophane structure composed of two aromatics units fixed in specific spatial arrangements, provided the overall structure lacks a symmetry plane. An early and instructive example was provided by Mayor and co-workers, who constructed asymmetric NDI-based cyclophanes **25** in which the face-to-face stacking of two aromatic units was enforced by a rigid bridging framework (Fig. 26).[119] In these systems, planar chirality does not originate from a local stereogenic element, but from the fixed spatial relationship between the two aromatic planes combined with asymmetric substitution that removes the mirror plane. Structural analysis confirmed that restricted bridge inversion prevents racemization, thereby stabilizing the planar chiral configuration. This study established a clear structural paradigm: planar chirality can be generated and maintained purely through geometric confinement within double-aromatic cyclophane scaffolds.

The structural concept of double-aromatic confinement was subsequently expanded into conjugated and stimuli-responsive systems. Takeuchi and co-workers reported a conjugated NDI-based cyclophane in which two co-facial NDI chromophores are bridged by 1,8-diethynylanthracene linkers, forming a rigid yet conformationally adaptable framework (Fig. 27).[120] The resulting **Cyclo-NDI** exists as an enantiomeric pair displaying pronounced circular dichroism and circularly polarized luminescence ($|g_{lum}| \approx 8 \times 10^{-3}$). Importantly, the system undergoes reversible interconversion between monomer-like and dimer-like conformations upon thermal modulation, leading to controllable variation in through-space π–π electronic coupling. In contrast to static planar chiral cyclophanes, this work demonstrates that planar chirality can be integrated with dynamic conformational switching, enabling reversible control over chiroptical output through modulation of inter-chromophoric communication.

Separately, the Tani group developed a class of carbazole-based [3.3](3,9)carbazolophanes.[121] In recent work, they

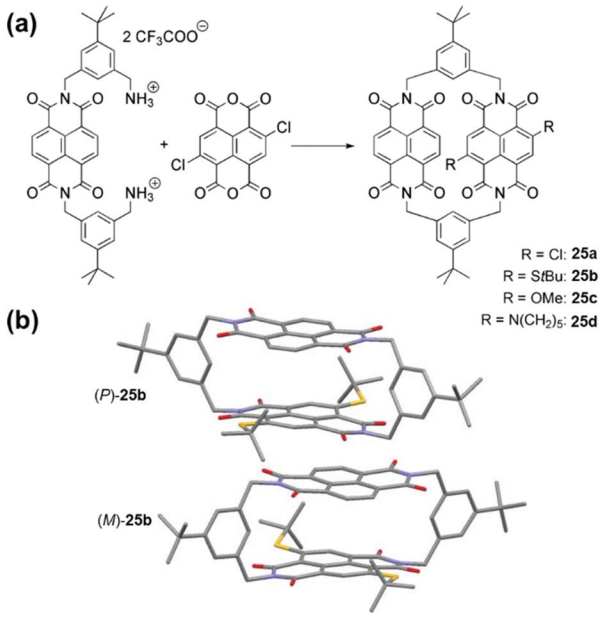

Fig. 26 (a) Synthesis of the asymmetric NDI-cyclophanes **25a–d**; (b) single-crystal structures of (*P*)-**25b** and (*M*)-**25b**. Reproduced from ref. 119. Copyright 2009 Royal Society of Chemistry.

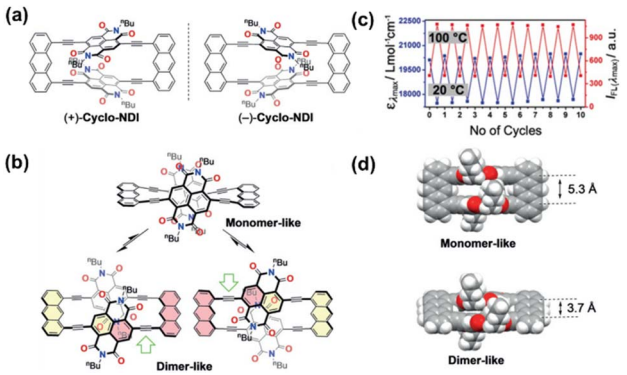

Fig. 27 (a) Chemical structures of **(+)-** and **(−)-Cyclo-NDIs**; (b) schematic illustration of conformational changes of **(+)-Cyclo-NDI**; (c) plots showing the reversibility of molar absorptivity and fluorescence intensity at the λ_{max} of **Cyclo-NDI** during 10 heating (100 °C)/cooling (20 °C) cycles in toluene.; (d) side views of calculated monomer-like and dimer-like structures of **(+)-Cyclo-NDI** with the interplanar distances between NDIs. Reproduced from ref. 120. Copyright 2019 Wiley-VCH.

achieved the first optical resolution of several [3.3](3,9)carbazolophane derivatives **CZ1–CZ3** (Fig. 28a).[122] These compounds display distinct signals in both CD and CPL spectra, with a high $|g_{lum}|$ as high as 0.013 (Fig. 28b). The study further revealed that the excellent chiroptical response of these planar chiral cyclophanes originates from the precise spatial arrangement of the two carbazole chromophores, thereby offering new molecular design principles for achieving high-performance chiroptical materials. The Tanaka group reported the stereoselective synthesis of [2.2]triphenylenophanes **26** incorporating PAHs (Fig. 29).[123] They achieved the diastereo- and enantioselective

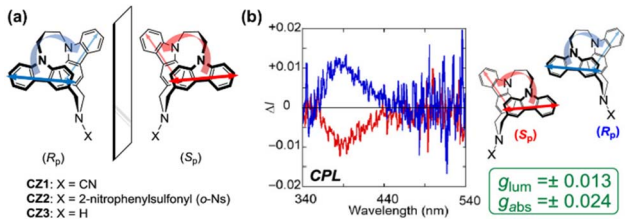

Fig. 28 (a) Structures of planar chiral [3.3](3,9)carbazolophanes (R_p)/(S_p)-**CZ1–CZ3**; (b) CPL spectrum of **CZ1**. Reproduced from ref. 122 Copyright 2020, American Chemical Society.

synthesis of planar chiral [2.2]triphenylenophanes through a base-mediated intermolecular macrocyclization followed by a rhodium/nickel-catalyzed intramolecular double [2 + 2 + 2] cycloaddition. This work demonstrates that transition-metal-catalyzed intramolecular double [2 + 2 + 2] cycloaddition serves as an excellent strategy for constructing cyclophanes containing functional PAHs.

Beyond thermally induced conformational dynamics, planar chiral cyclophanes can also undergo adaptive reconfiguration under supramolecular stimuli. Cheng and co-workers developed a family of naphtho[*n*,*n*]uril (**NGU[*n*,*n*]**) macrocycles that exhibit interconvertible R_p and S_p planar chiral conformations (Fig. 30).[124] In the case of **NGU[2,2]**, stepwise complexation with chiral amino acid derivatives perturbs the equilibrium among the planar chiral conformers in a binding-stoichiometry-dependent manner. Whereas formation of the 1 : 1 host–guest complex stabilizes the R_p conformer, further binding to generate the 1 : 2 complex shifts the equilibrium toward the S_p form, resulting in concentration-dependent inversion of CD signals. Notably, the coupling of sequential binding events with conformational interconversion produces temporal chiral inversion and overshoot phenomena, representing a supramolecular manifestation of allosteric regulation within a planar chiral macrocyclic framework.

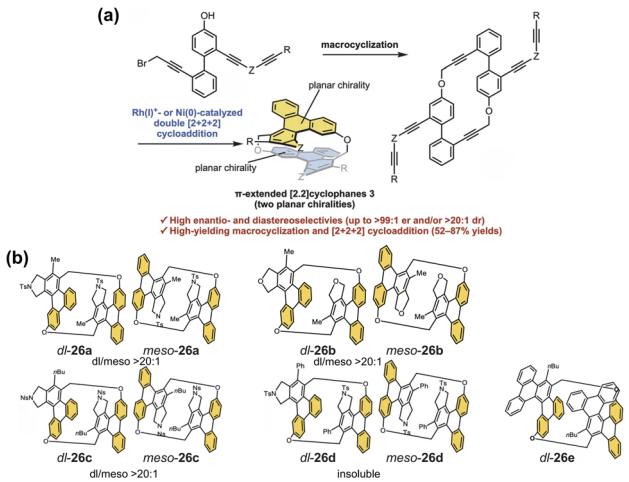

Fig. 29 (a) Schematic illustration of the stereoselective synthetic strategy for [2.2]triphenylenophanes; (b) structures of **26a–e**. Reproduced from ref. 123. Copyright 2023 Royal Society of Chemistry.

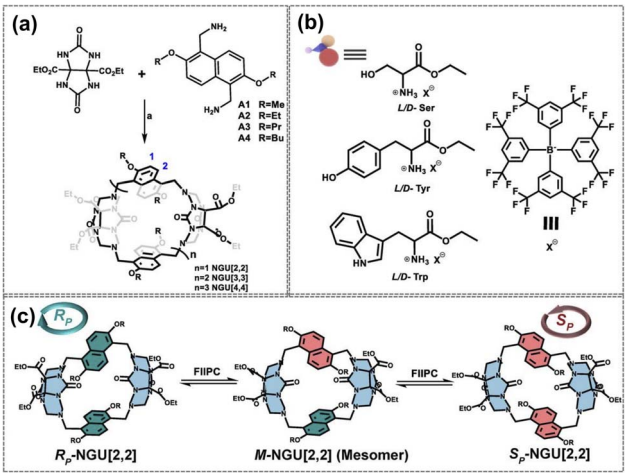

Fig. 30 (a) Chemical structures and synthetic route of NGU[*n*,*n*]s; (b) chemical structures of chiral guests; (c) schematic representation of the interconvertible conformations in R_p-NGU[2,2]. Reproduced from ref. 124. Copyright 2025 Wiley-VCH.

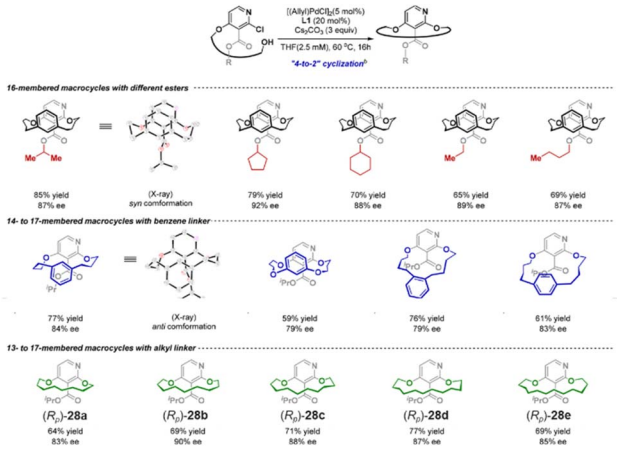

Fig. 32 Synthesis of various planar chiral metacyclophanes including compounds **28a–e**. Reproduced from ref. 129. Copyright 2023 American Chemical Society.

Planar chirality is not confined to double-aromatic cyclophanes. It can also arise when a single aromatic or heteroaromatic ring is bridged across non-adjacent positions, thereby preventing inversion through the ring plane. Ishida and co-workers provided an early demonstration of this principle by synthesizing a cyclophane-type imidazole **27** in which the C(2) and C(5) positions are connected by a decamethylene bridge (Fig. 31).[125] The short linker enforces differentiation of the two faces of the imidazole ring and suppresses rope-skipping motion, affording configurationally stable planar chiral enantiomers that were resolved by chiral HPLC. This example illustrates that planar chirality can be encoded within a single heteroaromatic framework without introducing classical stereogenic centers, highlighting the minimal structural requirements necessary for generating stable planar asymmetry.

With the progress of synthetic techniques, an increasing number of stereoselective synthetic strategies have been developed for such cyclic compounds,[126–128] significantly expanding the diversity of this class of compounds. For example, Li and colleagues developed an enantioselective Pd-catalyzed C–O bond-forming macrocyclization for the efficient construction of planar chiral metacyclophanes (Fig. 32).[129] This strategy employs 2,3,4-trisubstituted dichloropyridines and linkers to construct linear precursors. Under catalysis by a chiral Pd/JosiPhos complex, it successfully achieves intramolecular asymmetric coupling between the aryl chloride and the alcohol. This method affords a series of planar chiral cyclophanes with varying bridge lengths and substitution patterns in good yields (59–85%) and with high enantioselectivity (79–92% ee). The products include examples **28a–e**, which consist of only a single aromatic ring and a linker. This work opens an important pathway for constructing structurally diverse planar chiral molecules *via* catalytic asymmetric macrocyclization, paving the way for their application in the fields of catalysis and medicinal chemistry.

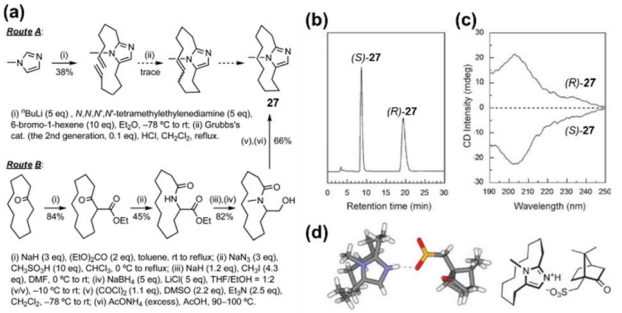

Fig. 31 (a) Synthesis of the cyclophane-type imidazole **27**; (b) chiral HPLC trace of **27**; (c) CD spectra of (*R*)- and (*S*)- **27** in H_2O; (d) X-ray crystal structure of the salt of (*S*)- **27** with (+)-10-camphorsulfonic acid. Reproduced from ref. 125. Copyright 2009 Royal Society of Chemistry.

While classical planar chirality typically derives from restricted inversion of aromatic planes, recent advances demonstrate that mechanical bonding offers an alternative pathway to encode planar asymmetry. Li and co-workers reported a series of "pretzelanes" (**29a–c**$^{n+}$) featuring a bridged [2]catenane core in which planar chirality arises from topological constraints rather than covalent bridge rigidity (Fig. 33).[130] In these structures, suppression of intramolecular pirouetting by the rigid bridge prevents restoration of mirror symmetry, yielding isolable enantiomers. Distinct from PCP-type systems, where planar chirality is geometrically imposed by through-bond constraints, pretzelanes derive configurational stability from mechanical interlocking. Moreover, the preorganized dual-cavity architecture enables efficient hydrophobic guest encapsulation in aqueous media, illustrating how mechanically induced planar chirality can simultaneously impart stereochemical definition and functional host properties.

A conceptually related yet mechanistically distinct example was reported by Tang, Zhang, Stoddart and co-workers, who achieved co-conformationally mechanical planar chirality

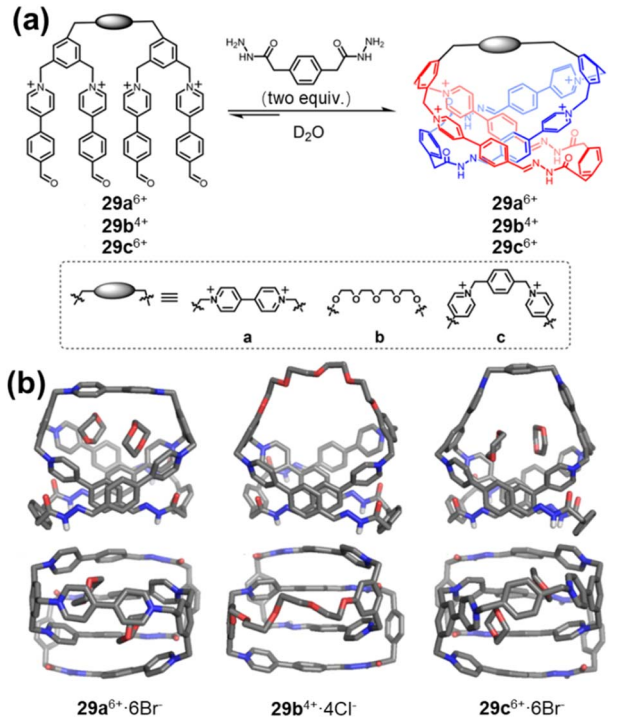

Fig. 33 (a) Synthesis and chemical structures of the pretzelanes $29a^{6+}$,$29b^{4+}$, and $29c^{6+}$; (b) side and top views of the solid-state structure of $29a^{6+}\cdot 6Br^{-}$,$29b^{4+}\cdot 4Cl^{-}$, and $29c^{6+}\cdot 6Br^{-}$. Reproduced from ref. 130. Copyright 2025 American Chemical Society.

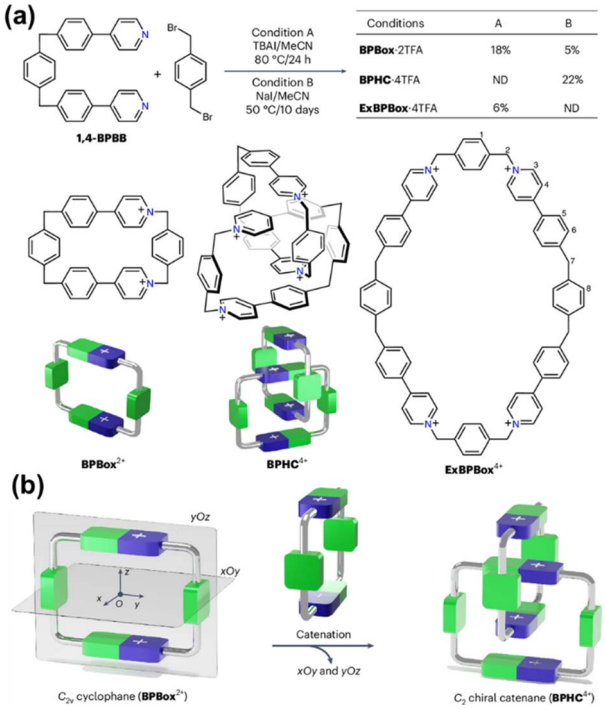

Fig. 34 (a) Synthesis of $BPBox^{2+}$, $ExBPBox^{4+}$ and $BPHC^{4+}$; (b) graphical representations of the C_{2v} cyclophane ($BPBox^{2+}$), and the chiral catenane ($BPHC^{4+}$). Reproduced from ref. 131. Copyright 2025 Springer-Nature.

through isostructural desymmetrization (Fig. 34).[131] Interlocking two symmetry-reduced yet achiral $BPBox^{2+}$ cyclophanes generates a C_2-symmetric catenane $BPHC^{4+}$ in which chirality emerges from loss of mirror symmetry upon catenation. Single-crystal analysis revealed racemic packing of enantiomeric co-conformations, while variable-temperature ^{1}H NMR studies demonstrated reversible pirouetting between them with a moderate activation barrier (16.4 kcal mol^{-1}). Importantly, introduction of chiral disulfonate anions biases the co-conformational equilibrium, inducing optical activity in solution and enabling crystallization of a single enantiomer. This system underscores that mechanical bonding not only encodes planar chirality but also permits its dynamic induction and external control, thereby extending planar chirality from a static geometric property to a tunable supramolecular parameter.

2.4 Chiral cyclophanes with multilayer chromophores

Multilayer cyclophanes are a special class of cyclophane molecules composed of multiple aromatic units stacked face-to-face. They represent structurally unique and functionally diverse systems in cyclophane chemistry. The interlayer interactions and overall conformations endow them with distinct photophysical properties and chiral expression.

The most typical examples belong to the class of multilayer PCPs.[132] Following early synthetic studies by Longone and Chow,[133,134] Nakazaki and coworkers successfully synthesized a series of chiral multilayer PCPs with defined absolute configurations (named [*n*]chochin, $n = 3$–6),[135] marking the first systematic introduction of chirality into multilayer cyclophane systems and achieving precise stereochemical control (Fig. 35). Subsequent investigations by Misumi and Otsubo into the spatial conformation, spectroscopic properties, and chemical reactivity of this system revealed that, besides strong through-space π–electron interactions, these molecules also exhibit unique chemical behavior.[136] For instance, due to the stabilization of the reaction transition state by through-space charge delocalization, bromination of the three-layer PCP ([3]chochin) preferentially occurs at the more sterically hindered but electron-rich inner benzene ring, with a reaction rate far exceeding that of the two-layer analog. These findings highlight the uniqueness of multilayer cyclophanes in terms of both structure and properties.

More complex multilayer chiral cyclophanes can be realized by designing extended π-systems, where the relative torsional arrangement between layers can induce overall helical chirality in the molecule. For example, Katoono, Suzuki, and colleagues designed a three-layer cyclophane **30** in which each stacked plane pair (top-middle, middle-bottom) can independently adopt either an (*M*)- or (*P*)-helical conformation (Fig. 36).[137] This results in a dynamic equilibrium between homochiral helical conformations [(*M*,*M*) or (*P*,*P*)] and an achiral conformation (*M*,*P*). The helicity of the molecule can be induced through complexation with chiral guests (*e.g.*, (*R*,*R*)- or (*S*,*S*)-**G5**), which bind to the bridging units *via* hydrogen bonding, thereby directing a specific helical sense. Notably, in the complexed state,

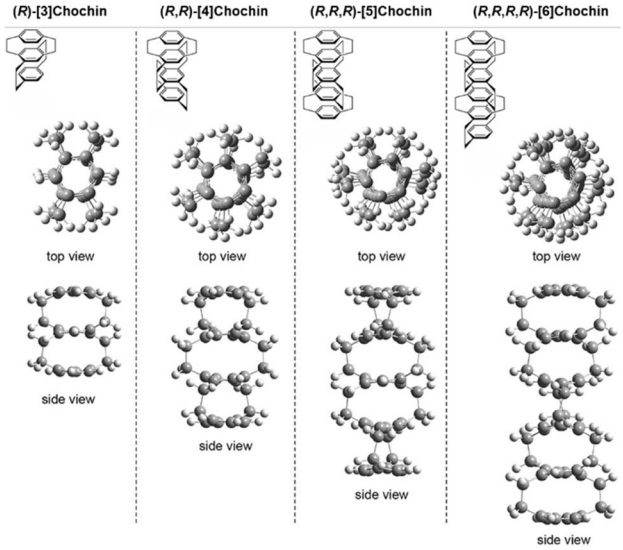

Fig. 35 Structures of multilayer PCPs with (*R*)-absolute configuration ([*n*]chochin, $n = 3$–6), showing front and side views. Reproduced from ref. 132. Copyright 2020 Sugiura.

the CD signal of the system anomalously strengthens considerably with heating. This work exemplifies the unconventional control over chiroptical properties achievable through the structural design of multilayer cyclophanes.

To further explore the intrinsic relationship between layer number and overall chiral conformation, Katoono and coworkers designed and synthesized a series of planar chiral cyclophanes with two (**31**), three (**32**), and four (**33**) layers (Fig. 37a).[138] These cyclophanes featured different substituents

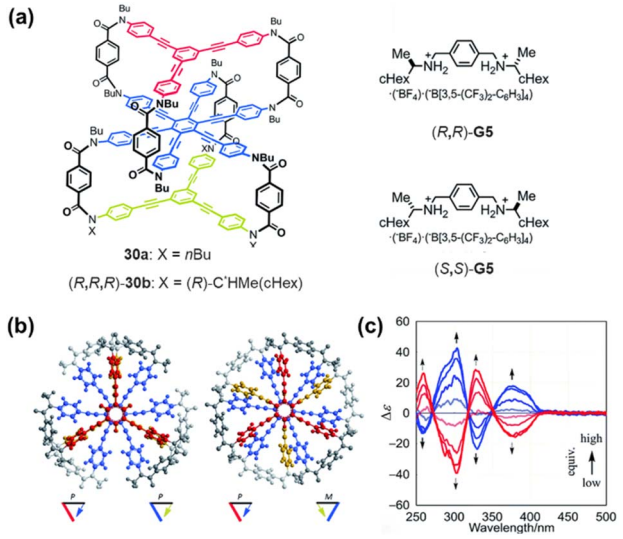

Fig. 36 (a) Structures of **30a**, (*R*,*R*,*R*)-**30b**, and chiral guest molecules (*R*,*R*)/(*S*,*S*)-**G5**; (b) computationally optimized predominant conformation of **30a′** (X = Me); (c) CD spectra of **30a** (7.1×10^{-5} M) in the presence of a chiral guest [3, 6, 8 and 12 equiv. of (*S*,*S*)-**G5** (red lines) or (*R*,*R*)-**G5** (blue lines)]. Reproduced from ref. 137. Copyright 2018, Royal Society of Chemistry.

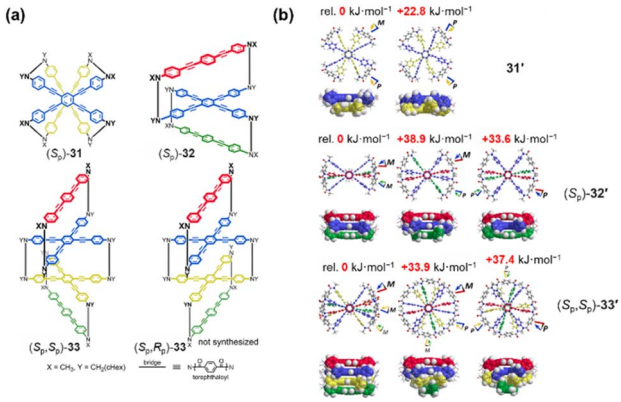

Fig. 37 (a) Structures of multilayer cyclophanes: two-layer (S_p)-**31**, three-layer (S_p)-**32**, and four-layer (S_p,S_p)/(S_p,R_p)-**33**; (b) computationally optimized energy-minimized structures of **31′**, (S_p)-**32′**, and (S_p,S_p)-**33′** (X = Y = CH_3), with the corresponding relative energies provided on the graphs (in kJ mol^{-1}). Reproduced from ref. 138. Copyright 2022 Royal Society of Chemistry.

on the bridging units (X = CH_3, Y = CH_2(cHex)). Computational predictions and CD spectroscopy indicated that the two-layer cyclophane **31** prefers a heterochiral form, whereas the three-layer **32** and four-layer **33** cyclophanes exhibit a strong preference for homochiral forms (Fig. 37b). This indicates an inherent molecular preference for a single helical sense (*e.g.*, *MM* or *MMM*), achieved through the intramolecular transmission of their inherent planar chirality. This work clearly elucidates, from a molecular design perspective, the relationship between layer number and the preferred overall helical conformation in multilayer cyclophanes.

Beyond single-layer architectures, multilayer chiral cyclophane-like architectures provide a powerful platform for hierarchical chirality expression and amplification. A representative related example is the tetraphenylethene-based octacationic spirobicycle **34** reported by Zhao and co-workers (Fig. 38a and b).[139] Its three-dimensional dual-cavity structure can encapsulate four d(GpC) dinucleotides in water to form a 1 : 4 host–guest complex—a double-layer G·C·G·C quadruplex (Fig. 38c and d). In this system, the cooperative hydrogen bonding, hydrophobic effects, and C–H···π interactions within the dual cavities collectively stabilize a multilayer hydrogen-bonded assembly, while the dynamically adaptive chirality of the host framework allows efficient chirality transfer and pH-dependent inversion of chiroptical signals.

3. Emerging functions and applications

The integration of pre-organized, three-dimensional cavities with exceptional chiroptical properties positions cyclophanes as uniquely powerful scaffolds in functional materials. These hybrid architectures merge the precise, guest-binding capabilities of macrocycles with the dissymmetric influence of chiral elements, enabling functions that are difficult to achieve with simpler molecular systems. This chapter will delve into how

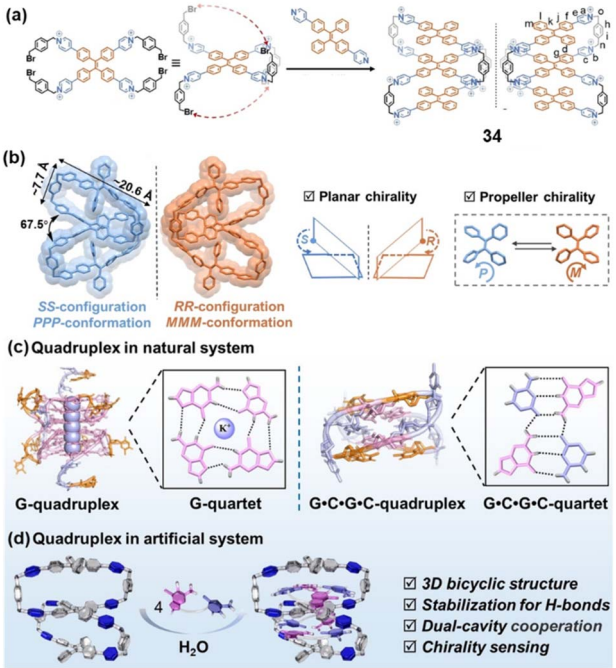

Fig. 38 (a) Synthesis route of **34**; (b) Enantiomeric crystal structures of **34**; (c) Representative conformational structures of G4 and G·C·G·C quadruplex; (d) biomimetic hydrogen-bonded G·C·G·C quadruplex within a spirobicyclic compound. Reproduced from ref. 139. Copyright 2024 Wiley-VCH.

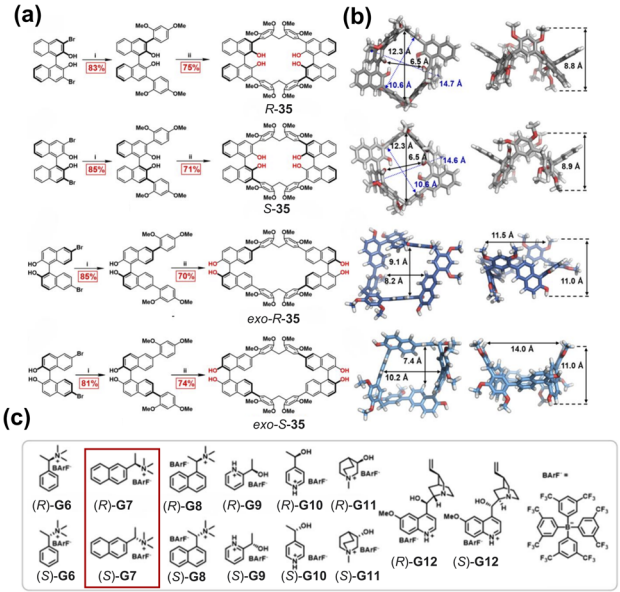

Fig. 39 (a) Synthesis of *R*/*S*-**35** and *exo*-*R*/*S*-**35**; (b) single-crystal structure of *R*/*S*-**35** and computationally optimized structure of *exo*-*R*/*S*-**35**; (c) structures of chiral guest molecules, with the guest pair [(*R*)/(*S*)-**G7**] showing the highest K_S/K_R ratio indicated in the figure. Reproduced from ref. 140. Copyright 2024 American Chemical Society.

these sophisticated designs are translated into practical and emerging applications across several advanced fields. In enantioselective recognition, the chiral and confined cavities act as selective hosts, discriminating between molecular enantiomers for sensing and purification. In asymmetric catalysis, cyclophane-based catalysts leverage their cavities to create highly stereocontrolled microenvironments, facilitating reactions with superior enantioselectivity. Finally, in chiral optical materials, their intrinsic and tunable chiroptical responses are harnessed for next-generation technologies such as CPL. By examining specific case studies and design principles, we will illustrate how the molecular elegance of cyclophanes is being transformed into tangible functional advantages.

3.1 Enantioselective recognition

Enantioselective recognition is one of the most fundamental functions of chiral cyclophanes and is very important in fields like chiral sensing, separation, and analysis. Chiral cyclophanes, with their adjustable cavity size, shape, and functionalizable inner walls, provide an ideal solution for efficient and highly selective chiral recognition. They can excellently identify a variety of chiral guests as highlighted in several case studies from the previous section.[63,99]

Li's research group has developed a series of chiral cyclophanes based on the BINOL skeleton that exhibit outstanding enantioselective recognition. They initially prepared two pairs of chiral cyclophanes, *R*/*S*-**35** and *exo*-*R*/*S*-**35**, *via* a straightforward two-step reaction (Fig. 39a and b).[140] These compounds could be purified using silica gel column chromatography without the need for chiral separation. Among them, the internally hydroxyl-directed cyclophane *R*/*S*-**35** achieved highly selective recognition of chiral ammonium salts, with the enantioselectivity ratio (K_S/K_R) reaching up to 13.2 (Fig. 39c). The combination of straightforward synthesis and high selectivity renders this system directly applicable to chiral recognition and separation.

In subsequent work, They further refined the cyclophane structure by introducing a benzothiadiazole unit to enrich the binding sites, yielding a new pair of chiral cyclophanes *R*/*S*-**36** (Fig. 40a).[141] This design retained the inwardly directed hydroxyl groups while incorporating rotatable S/N atoms as additional recognition sites. These cyclophanes could also be purified without chiral resolution and were successfully applied to the highly enantioselective recognition of chiral pharmaceutical intermediates such as (*R*)-**G14**, achieving K_S/K_R value of 9.6 (Fig. 40d). Theoretical calculations revealed that the high selectivity originates from favorable spatial complementarity between host and guest, along with a synergistic combination of multiple noncovalent interactions, including hydrogen bonding, π–π donor–acceptor interactions, and C–H···π interactions. Collectively, these studies demonstrate the versatility and application prospects of chiral cyclophanes in enantioselective recognition, offering a new approach for efficient separation of chiral pharmaceutical intermediates.

However, achieving highly enantioselective recognition in aqueous media has remained a significant challenge in the field. The team of Jiang addressed this issue through ingenious biomimetic design, synthesizing a class of chiral naphthotubes

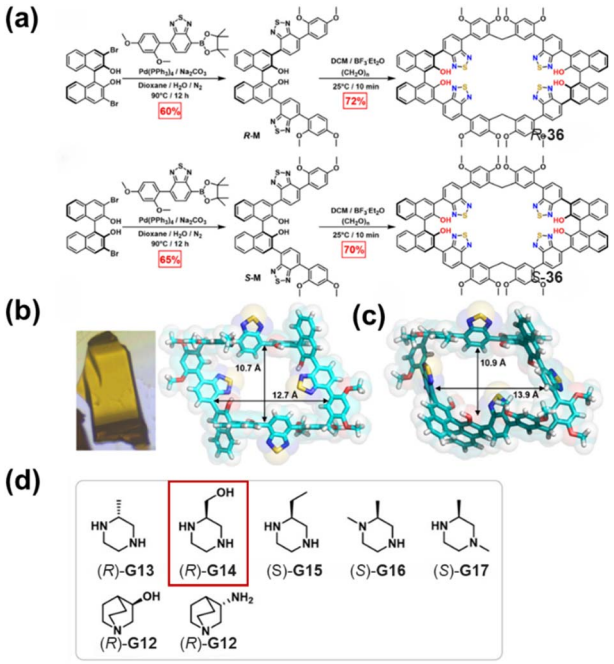

Fig. 40 (a) Synthesis of *R*/*S*-**36**; (b) photograph of single crystals and single-crystal structure of *R*-**36**; (c) computationally optimized structure of *S*-**36**; (d) structures of chiral guest molecules, with the guest [(*R*)-**G14**] showing the highest K_S/K_R ratio indicated in the figure. Reproduced from ref. 141. Copyright 2025 American Chemical Society.

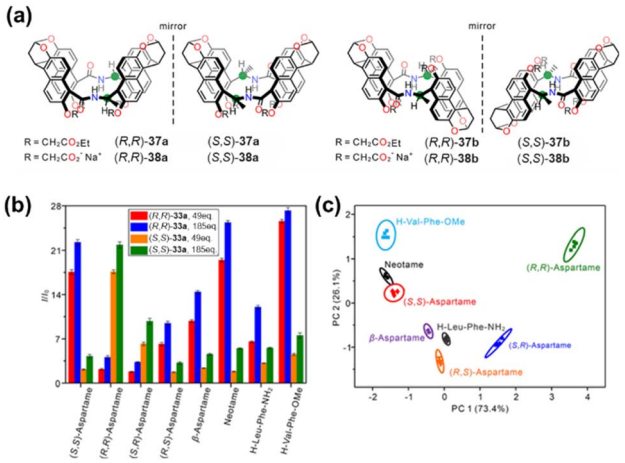

Fig. 41 (a) Structures of chiral naphthotubes **37** and **38**; (b) fluorescence responses of (*R*,*R*)-**38a** and (*S*,*S*)-**38a** (0.01 mM) at 404 nm (λ_{ex} = 356 nm) upon addition of the eight sweetener-related molecules (49 and 185 equiv.) in phosphate buffer (50 mM, pH = 7.40, 25 °C). Each host shows a different fluorescence response, and these responses can be subjected to PCA to differentiate the sweetener molecules and the related molecules. The error bars on the bar graph are standard deviations of the five individual responses. (c) Score plot obtained by PCA of the analytes using naphthotubes **38a**. Ellipsoids on the scatter plot are drawn at 95% confidence. Sweetener molecules and the related molecules are well separated from each other. Reproduced from ref. 45. Copyright 2024 American Chemical Society.

37 and **38** (Fig. 41a).[45] Their chiral centers are adjacent to amide groups oriented toward the cavity interior, mimicking structural features commonly found in biological receptors. These water-soluble chiral cyclophanes can selectively recognize up to 90 types of chiral guest molecules in water, including various small organic molecules and pharmaceutical compounds. The enantioselectivity factor for neotame reached as high as **34**. Mechanistic studies revealed that this high selectivity originates from the accumulation of subtle differences in multiple non-covalent interactions within the hydrophobic cavity. Furthermore, these chiral naphthotubes, combined with fluorescence response and principal component analysis (PCA), successfully distinguished all four stereoisomers of aspartame and their analogs (Fig. 41b and c). The high enantioselectivity and unprecedented broad substrate adaptability shown by this system provide a strong basis for developing next-generation applications in aqueous-phase chiral sensing and separation.

3.2 Catalytic reactions and asymmetric catalysis

In the field of catalytic applications, chiral cyclophanes enable efficient catalysis by utilizing their unique cavities to provide precise preorganization and stabilization for reactants and transition states. For instance, Sun and colleagues designed a highly efficient catalytic system that synergizes with Pd(II), based on a novel chiral bis(*N*-heterocyclic carbene) (NHC) precursor (Fig. 42a).[142] Using sodium formate as a hydrogen source under mild conditions, this system achieved hydrodehalogenation of various aryl halides, with conversion exceeding 99% for substrates like 1,2-dichlorobenzene (Fig. 42b). The specific spatial arrangement of the imidazolinium protons on both sides of the cyclophane's cavity reduces steric hindrance and creates a synergistic effect. This drastically minimizes the generation of chlorobenzene intermediates during the dehalogenation of polychlorinated benzenes. This NHC precursor shows promise for application in further catalytic reactions, such as the debromination of bromobenzene, potentially opening new avenues for coupling reactions.

In the more challenging realm of asymmetric catalysis, the value of chiral cyclophanes is even more pronounced, especially

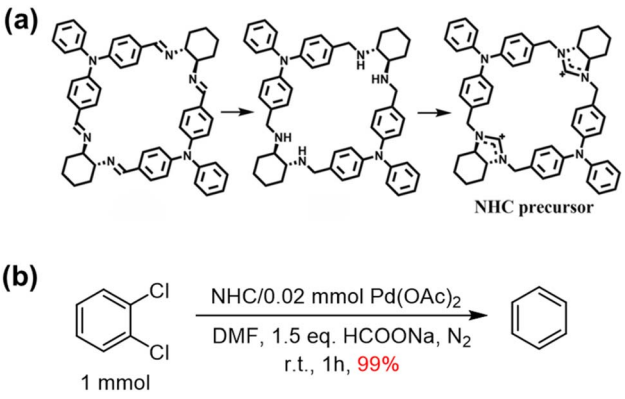

Fig. 42 (a) Synthesis of the NHC precursor; Reproduced from ref. 142. Copyright 2023 Elsevier B.V. (b) Reaction conditions for the hydrodehalogenation of 1,2-dichlorobenzene catalyzed by the NHC–Pd(II) complex.

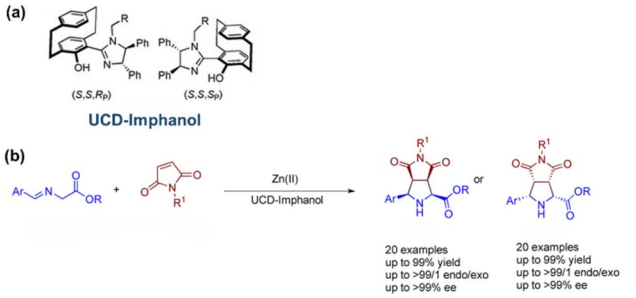

Fig. 43 (a) Structures of a pair of diastereomers of UCD-Imphanol; (b) schematic of the highly enantioselective [3 + 2] azomethine ylide cycloaddition catalyzed by the UCD-Imphanol/Zn(II) complex. Reproduced from ref. 145. Copyright 2022 Wiley-VCH.

as chiral catalysts based on PCP frameworks have begun to make their mark in this domain.[143,144] Building upon these early explorations, Guiry *et al.* prepared a novel class of imidazolinyl-[2.2]paracyclophanol (UCD-Imphanol) ligands (Fig. 43a).[145] The catalytic system formed by these ligands with Zn(II) demonstrated outstanding performance in asymmetric [3 + 2] azomethine ylide cycloaddition reactions, affording the target chiral pyrrolidine derivatives with excellent results: up to >99% yield, >99/1 *endo*/*exo* selectivity, and >99% ee (Fig. 43b). Mechanistic studies revealed that the planar chirality element within the ligand is the dominant factor governing the asymmetric induction. Subsequently, Guo *et al.* performed innovative design on the PCP framework, developing a new class of chiral indenyl ligands based on [2.2]benzoindenophane (Fig. 44).[146] The catalyst formed by their coordination with rhodium afforded remarkable enantiocontrol in two distinct asymmetric C–H activation reactions. Not only did this catalyst facilitate the asymmetric annulation of *O*-boc hydroxybenzamides with alkenes, constructing chiral dihydroisoquinolinones with up to 97% yield and 98% ee, but it also successfully catalyzed the asymmetric C(sp^2)-H activation/oxidative coupling of carboxylic acids with alkynes. This reaction afforded axially chiral isocoumarins with up to 99% yield and 94% ee. This work represents the first reported example of constructing isocoumarins *via* enantioselective transition-metal-catalyzed C(sp^2)-H activation/oxidative coupling of benzoic acids with internal alkynes. Owing to its straightforward synthesis, high tunability, and exclusive face selectivity in coordination, this system holds broad application prospects in catalytic asymmetric C–H activation and other asymmetric reactions.

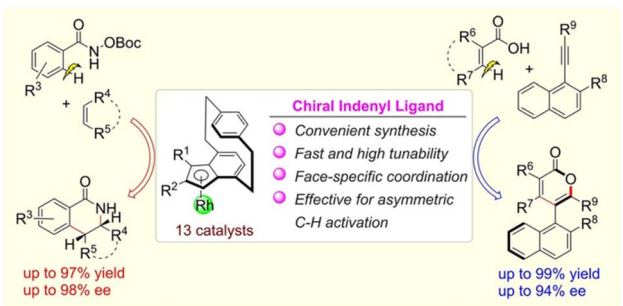

Fig. 44 Schematic illustration of the novel chiral indenyl rhodium catalysts based on [2.2]benzoindenophane for asymmetric C–H activation to construct dihydroisoquinolinones and axially chiral isocoumarins. Reproduced from ref. 146. Copyright 2024 Wiley-VCH.

3.3 Circularly polarized luminescence and chiral optical materials

Chiral cyclophanes are demonstrating exceptional application capability in the field of advanced optical materials, particularly in CPL and chiral optical materials. It is well known that CPL materials hold broad prospects for applications such as information encryption storage and biological probes. Due to their precisely tunable luminescent units and chiral sources, chiral cyclophanes are capable of effectively transferring chiral information to the luminescent centers, thereby generating strong CPL signals. This makes them an ideal platform for constructing high-performance CPL materials.

A seminal example demonstrating the integration of planar chirality, TADF, and circularly polarized luminescence (CPL) within a single cyclophane framework was reported by Zysman-Colman and co-workers.[147] In this work, a carbazolophane donor derived from a [2.2]PCP scaffold was incorporated into a donor–acceptor triazine emitter (Fig. 45a). The sterically encumbered and rigid cyclophane framework enforced a larger torsional angle between the donor and the aryl bridge, reducing the singlet–triplet energy gap (ΔE_{ST}) from 0.32 eV in the reference carbazole analogue **CzPhTrz** to 0.16 eV in **CzpPhTrz** (**39**), thereby efficiently activating the TADF channel. Importantly, the inherent planar chirality of the [2.2]paracyclophane enabled enantiomerically pure emitters that exhibited mirror-image CD and CPL spectra, with $|g_{lum}|$ values of approximately 1.3×10^{-3}. Furthermore, the sky-blue OLED fabricated using rac-CzpPhTrz achieved a maximum external quantum efficiency of 17% (Fig. 45c), representing the first example of an electroluminescent device incorporating a [2.2]paracyclophane moiety.

Building upon molecular-level integration of planar chirality and TADF, further advances have demonstrated that three-dimensional donor–acceptor architectures can provide additional control over excited-state interactions. In a recent report from Zhang's group, a chiral donor–acceptor cage (**DA-2**) was developed as the first example of a CP-TADF organic cage (Fig. 46a).[148] Single-crystal analysis revealed a propeller-like three-dimensional framework in which donor and acceptor units are spatially aligned with an intramolecular distance of 3.7 Å (Fig. 46b), enabling efficient through-space charge transfer (TSCT). Photophysical studies demonstrated a remarkably small singlet–triplet energy gap ($\Delta E_{ST} = 0.051$ eV) in solution, confirming efficient TADF. Importantly, theoretical analysis of the excited-state transition density showed quasi-parallel transition electric and magnetic dipole moments, a structural feature that maximizes the luminescence dissymmetry factor (Fig. 46c). As a result, DA-2 exhibited $|g_{lum}|$ values up to 2.1×10^{-3} in PMMA films with a photoluminescence quantum yield of 32%. These studies illustrate two complementary approaches for constructing CP-TADF systems: one based on planar chiral

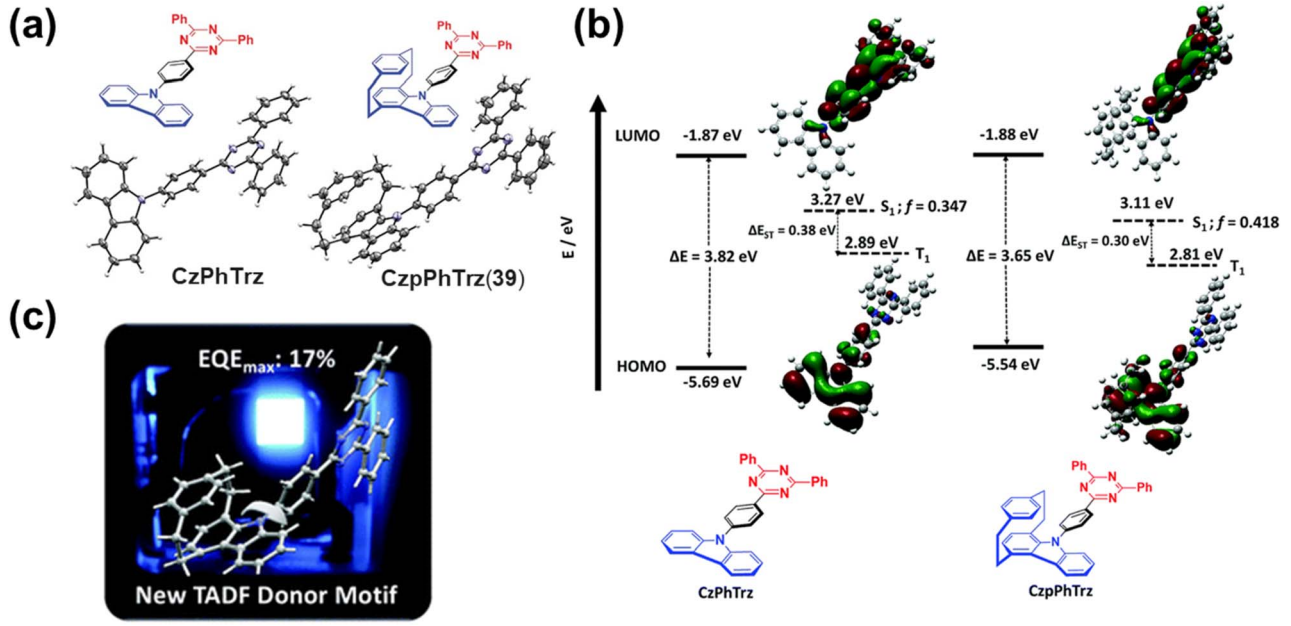

Fig. 45 (a) Molecular structures of **CzPhTrz** and (*rac*)-**CzpPhTrz**; (b) DFT [PBE0/6-31G(d,p)] calculated ground and TDA-based excited state energies and electron density distributions of the HOMOs and LUMOs of **CzPhTrz** and **CzpPhTrz**, *f* is the oscillator strength; (c) schematic of the sky-blue OLED fabricated using rac-**CzpPhTrz**. Reproduced from ref. 147. Copyright 2019 Royal Society of Chemistry.

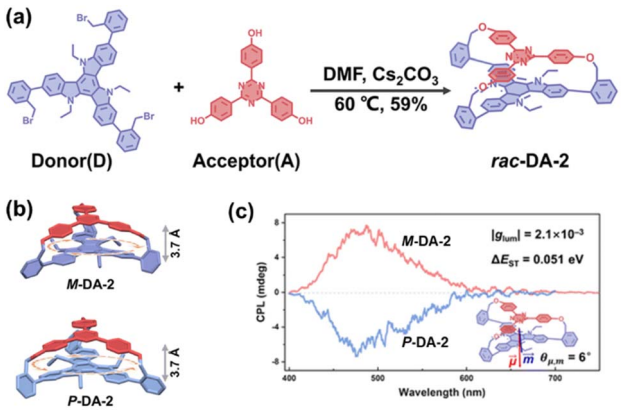

Fig. 46 (a) Synthetic route of **DA-2**; (b) single-crystal structure of a pair of **DA-2** enantiomers; (c) CPL spectra and some physical properties of **DA-2**. Reproduced from ref. 148. Copyright 2024 Royal Society of Chemistry.

cyclophane scaffolds that modulate torsional geometry and excited-state energetics through through-bond effects, and the other relying on three-dimensional cage architectures that promote through-space charge transfer and favorable dipole alignment. Both strategies highlight how precise spatial organization within constrained frameworks can simultaneously reduce ΔE_{ST} and generate efficient circularly polarized emission.

Barendt *et al.* presented a class of configurationally stable bis-PBI cyclophanes (**40-*MM*** and **40-*PP***) connected at the bay positions (Fig. 47a).[149] Their chirality-locked structures enable the formation of single-crystalline materials exhibiting strong CPL emission through self-assembly. This substitution pattern of PBI provides a new strategy for the rational design of H-type, J-type, and mixed H/J-type self-assembled materials, offering important insights for optimizing chiroptical properties as well as charge/energy transport characteristics. Significantly, this work accomplished the first CPL laser scanning confocal microscopy (CPL-LSCM) imaging analysis of chiral organic single crystals. The authors established a quantitative analysis method based on enantiomer discrimination using differential

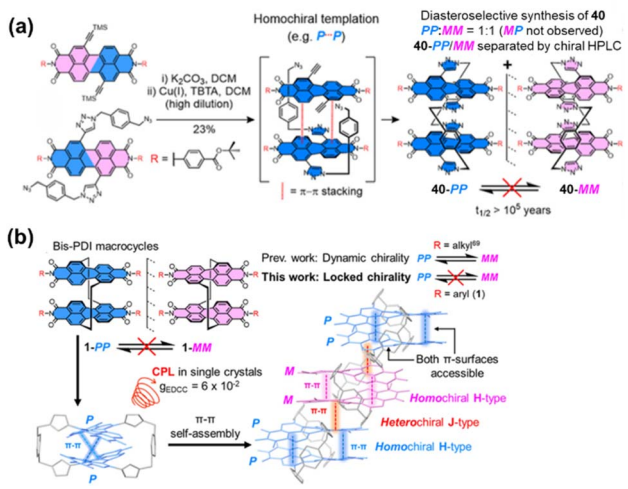

Fig. 47 (a) Synthesis of bis-PBI cyclophanes **40-*MM*** and **40-*PP***; (b) Chirally locked bis-PDI cyclophane **40** facilitates π−π stacking on both PDI π-surfaces, generating CPL in single crystals and enabling concurrent formation of H- and J-type aggregates. Reproduced from ref. 149. Copyright 2024 American Chemical Society.

contrast (EDCC), and quantified the circular polarization degree of the emitted light by calculating the EDCC asymmetry factor ($g_{EDCC} = 6 \times 10^{-2}$, physically analogous to g_{lum}), thereby providing a powerful tool for characterizing chiral single-crystalline materials at the microscopic scale (Fig. 47b).

PBI-based chiral cyclophanes also show promise as chiroptical switches—an important class of chiroptical materials capable of altering the sign or intensity of their CD or CPL signals in response to external stimuli. They further developed a bis-PBI cyclophane **41** that combines configurational stability with conformational flexibility, which facilitates solvent-induced switching of CD and multiphoton excitation CPL (MP-CPL) signals (Fig. 48).[150] This system represents the first organic emitter demonstrating MP-CPL switching behavior, reversibly modulating CPL signal amplitude in toluene and chlorinated solvents. Since multiphoton excitation employs near-infrared light, which offers superior tissue penetration and reduced cytotoxicity, it overcomes the limitations associated with UV or visible light excitation, thereby holding more advantageous for biological imaging applications

Following the realization of dual responsiveness to solvent stimuli, the research group further deepened their investigation into chiroptical switches by designing a triple chiroptical switch system. The team synthesized a novel class of bis-PBI cyclophanes **42** incorporating L/D-valinol at the imide positions, successfully transferring and converting the central chirality of the amino acid into helical chirality within the PBI dimer.[151] The most remarkable feature of this molecule lies in its unprecedented function as a triple chiroptical switch: using achiral solvents (such as chloroform and water) as stimuli enables reversible inversion of the CD and CPL signal signs; simultaneously, molecular recognition between the cyclophane and PAH guests allows modulation of CD signal intensity and complete shut-off of CPL emission. Consequently, this study

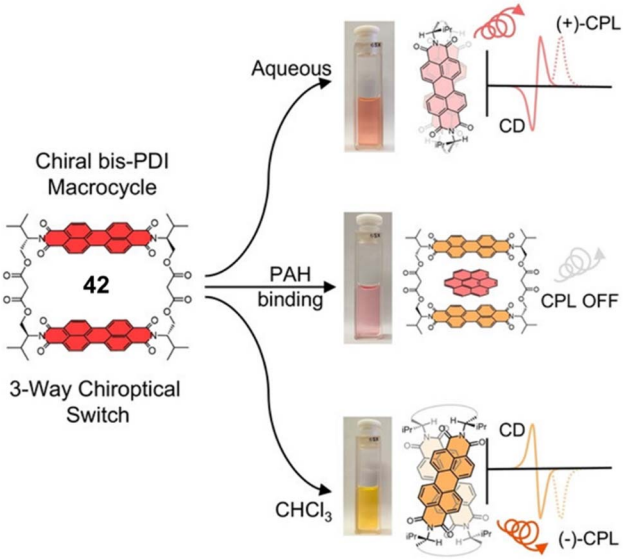

Fig. 49 Schematic illustration of the unique three-way chiroptical switch (+/−/off) behavior exhibited by the bis-PBI cyclophane **42**. Reproduced from ref. 151. Copyright 2025 Wiley-VCH.

represents the first implementation of integrated control over both sign inversion and intensity switching of CPL signals within a discrete organic molecular system in solution, achieving a unique three-way CD/CPL switch (Fig. 49). This intelligent molecular system, capable of generating distinct chiroptical responses to multiple achiral stimuli, holds considerable promise for in advanced chemical sensing, secure information encryption, and multistate logic operations.

Planar chiral pyrenophanes, as a class of structurally rigid chiral luminescent systems, showcase considerable promise in CPL and the emerging field of circularly polarized

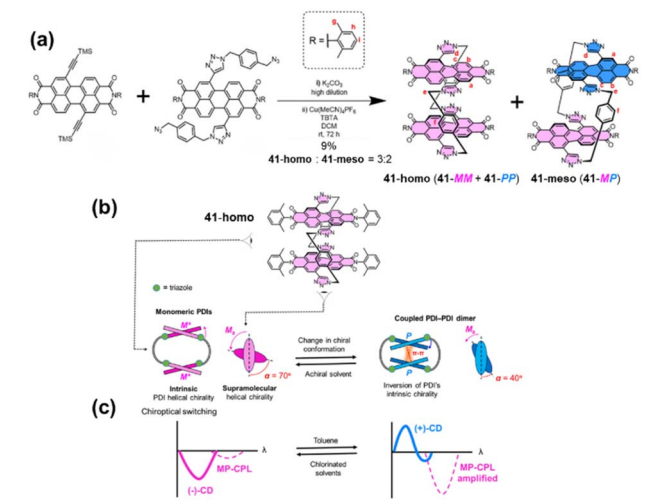

Fig. 48 (a) Synthesis of bis-PBI cyclophanes **41-homo** and **41-meso**; (b) Achiral stimulus-induced conformational change in the chiral bis-PBI cyclophane **41-homo**; (c) solvent-induced switching of CD and MP-CPL signals. Reproduced from ref. 150. Copyright 2025 Wiley-VCH.

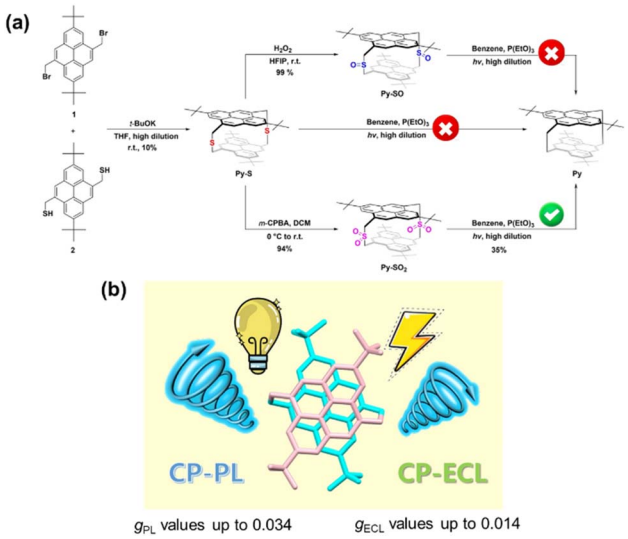

Fig. 50 (a) Synthesis of planar chiral pyrenophanes **Py-S**, **Py-SO**, **Py-SO$_2$**, and **Py**; (b) these pyrenophanes exhibits stable and intense CP-PL and CP-ECL properties. Reproduced from ref. 152. Copyright 2025 Wiley-VCH.

electrochemiluminescence (CP-ECL). Wang and colleagues synthesized a series of novel pyrenophanes (**Py-S**, **Py-SO**, **Py-SO$_2$**, and **Py**) with tunable bridging structures (Fig. 50a).[152] Owing to their rigidly locked pyrene dimeric architecture, these systems not only achieve highly efficient circularly polarized photoluminescence (CP-PL) with a luminescence dissymmetry factor (g_{PL}) as high as 0.034 but also exhibit remarkable stability across various solvents, temperatures, and concentrations. This makes them a reliable material platform with great promise for practical applications such as chiral sensing. Particularly noteworthy is their excellent CP-ECL performance, with a g_{ECL} value reaching 0.014 (Fig. 50b), ranking among the highest reported to date. This CP-ECL capability expands the application scope of chiral cyclophanes in electrochemiluminescent devices, highlighting both its fundamental research significance and practical application prospects.

Chiral cyclophanes have recently showcased unique utility in emerging areas such as organic optoelectronics. For example, Shimada and coworkers developed a series of planar chiral tetrasila[2.2]cyclophanes (**43a–i**) with remarkable applications in organic optoelectronic devices (Fig. 51a).[153] The donor–acceptor tetrasila[2.2]cyclophanes (**43e–h**) exhibit green emission originating from intramolecular charge transfer. Notably, compound **43f** shows strong solid-state luminescence ($\Phi = 0.49$) due to suppressed intermolecular π–π stacking. Compound **43i** displays distinct CPL signals in solution with a luminescence dissymmetry factor of approximately 2×10^{-3} at 500 nm, a value comparable to those of some high-performance low-molecular-weight chiral emitters. More significantly, this class of cyclophanes can serve as emitting layer dopants in organic light-emitting diodes (OLEDs). By doping the donor–acceptor compound **37f** into a dPVBi host matrix, the researchers fabricated a multilayer OLED that produces green emission at 495 nm with a maximum external quantum efficiency of 0.36% (Fig. 51b). These results confirm the feasibility of using tetrasila[2.2]cyclophanes in electroluminescent devices and highlight their potential for practical applications as emitting dopants in solid-state lighting and display technologies.

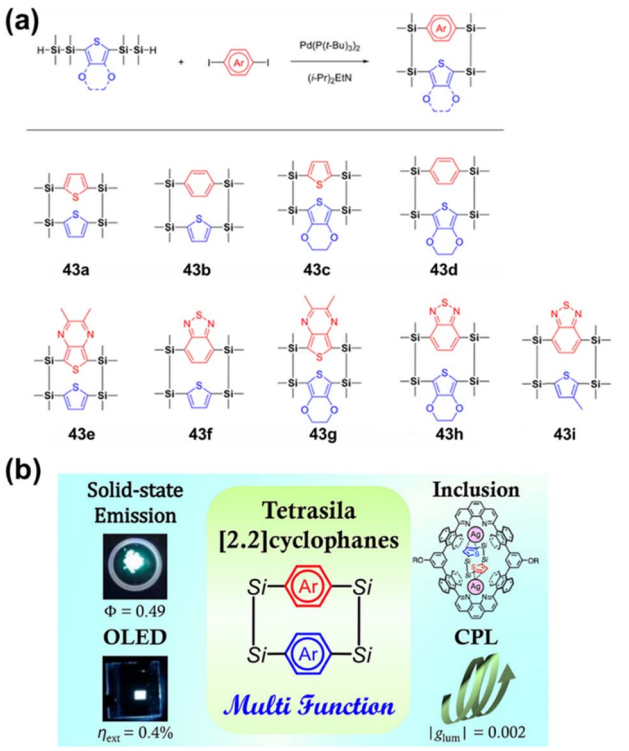

Fig. 51 (a) Synthesis of planar chiral tetrasila[2.2]cyclophanes **43a–i**; (b) schematic illustration of the luminescence properties of tetrasila[2.2]cyclophanes, highlighting their solid-state emission and CPL characteristics with potential applications in OLED. Reproduced from ref. 153. Copyright 2017 American Chemical Society.

Wang and colleagues described a class of planar chiral charge-transfer cyclophanes whose tightly π-stacked structure facilitates efficient intramolecular charge transfer and endows them with remarkable photothermal properties (Fig. 52a).[154] The enantiomer **C8BDT-NDI** exhibits a distinct chirality-dependent photothermal response under circularly polarized light irradiation: when exposed to left-handed circularly polarized light, the (*R*)-enantiomer reaches a higher equilibrium temperature than its (*S*)-counterpart. This differential response to chiral light establishes a foundation for its application in the field of novel chiral photothermal materials. Furthermore, this class of chiral cyclophanes displays effective chiral transfer and amplification in supramolecular assembly. For instance, (*R*)- and (*S*)–**C8DN-NDI** self-assemble in THF-H_2O mixed solvents into well-defined nanohelical structures with specific *M*- or *P*-handedness, respectively, achieving efficient transfer and amplification of chirality from molecular planar chirality to supramolecular helical chirality (Fig. 52b). Such chiral

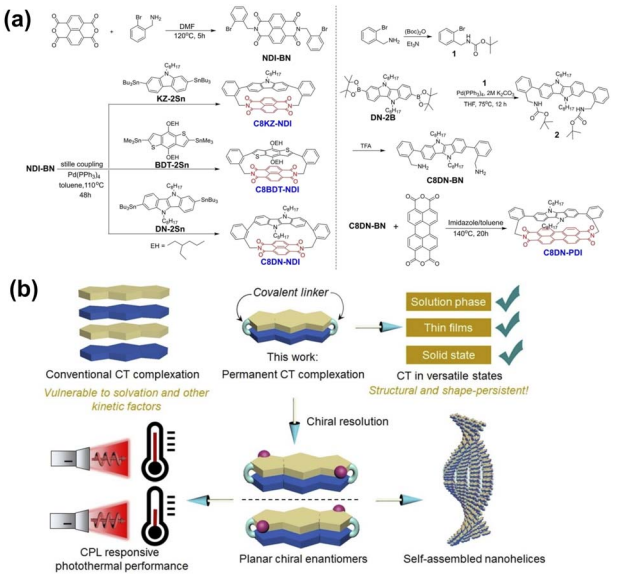

Fig. 52 (a) Synthesis of planar chiral charge-transfer cyclophanes **C8KZ-NDI**, **C8BDT-NDI**, **C8DN-NDI**, and **C8DN-PDI**; (b) schematic illustration of the photothermal properties and self-assembly behavior of this class of cyclophanes, demonstrating their chirality-dependent photothermal response and the formation of nanohelical structures. Reproduced from ref. 154. Copyright 2024 Wiley-VCH.

supramolecular assembly behavior provides a new molecular platform for constructing advanced chiral functional materials.

These investigations in fields such as organic optoelectronics and chiral photothermal materials convincingly show that chiral cyclophanes, as highly tunable functional platforms, possess promise that remains largely untapped. These studies, transcending conventional boundaries, open up broad prospects for their innovative applications in future multifunctional materials and devices.

4. Summary and outlook

In conclusion, chiral cyclophanes represent a remarkable fusion of supramolecular topology, precise structural engineering, and chiral functionality. By integrating well-defined, preorganized cavities with tailored asymmetry, these macrocycles offer a powerful platform for amplifying and expressing chirality. Their unique properties stem from the exquisite control over the spatial arrangement of chromophores, *i.e.*, governing their relative orientation, distance, and dissymmetry, which collectively enable exceptional chiral recognition, catalysis and distinct chiroptical behaviors, such as intense circularly polarized luminescence. This review systematically summarizes the research progress in the field of chiral cyclophanes according to the origin of chirality, whether from chiral chromophores, chiral linkers, inherent planar chirality, or stacked multilayer architectures, which provides a logical and instructive framework. This structure-based classification not only clarifies the diverse design principles but also serves as a practical guide for the rational design of new systems with targeted properties. As a result, chiral cyclophanes are demonstrating ever-expanding functionalities, showing significant promise in cutting-edge applications such as high-performance CPL materials, enantioselective sensing, asymmetric catalysis, controlled supramolecular assembly, and biomedicine.

Despite these notable achievements, the field still faces several challenges and development opportunities. First, in synthetic chemistry, the efficient and highly enantioselective synthesis of complex cyclophanes, such as those with specific planar chirality or containing functionalized units, remains a daunting task. Future progress relies on designing more universal and precise catalytic cyclization strategies—for instance, expanding the application of asymmetric C–H activation, RCM, *etc.*, in cyclophane construction—to attain precise control over the size, shape, and absolute configuration of cyclophanes. Secondly, research into the behavior and mechanisms of chiral cyclophanes in supramolecular assembly is at a critical juncture. Core difficulties persist in understanding how molecular chirality is precisely transmitted and amplified into supramolecular aggregates, and in deeply investigating the thermodynamic and kinetic controlling factors, solvent effects, and chiral cooperative effects during assembly that ultimately determine the macroscopic chiroptical properties and functions. Moreover, in functional application, cyclophane chemistry currently faces issues such as relatively limited functionality and insufficient maturity in translating unique properties into practical applications, leaving its potential in frontier areas far from fully realized. Consequently, future research will continue to delve deeply into the design, synthesis, and functional applications of chiral cyclophanes.

In conclusion, chiral cyclophanes represent a bridging research field that connects fundamental molecular design with cutting-edge functional applications and is currently in a stage of rapid advancement. We are convinced that through innovations in synthetic methodologies, deepening mechanistic studies, and enhanced interdisciplinary collaboration, chiral cyclophanes might foster the development of next-generation functional macrocycles. The journey from beautifully intricate structures to sophisticated functional systems is well underway, promising exciting discoveries and applications in the years to come.

Author contributions

Conceptualization, G. Ouyang; writing – original draft, Y. Zhang, H. Jia; writing – review & editing, G. Ouyang, L. Xu and M. Liu; supervision, G. Ouyang and L. Xu.

Conflicts of interest

There are no conflicts to declare.

Data availability

Data for this review article are available from the references.

Acknowledgements

The authors are grateful for the financial support from the National Natural Science Foundation of China (22322207 and 92356307), the National Key Research and Development Program of China (2022YFA1204402).

Notes and references

1 D. Ramaiah, P. P. Neelakandan, A. K. Nair and R. R. Avirah, *Chem. Soc. Rev.*, 2010, **39**, 4158–4168.
2 G. Chehardoli and A. Bahmani, *Supramol. Chem.*, 2019, **31**, 221–238.
3 Z. Qi, Y. Qin, J. Wang, M. Zhao, Z. Yu, Q. Xu, H. Nie, Q. Yan and Y. Ge, *Front. Chem.*, 2023, **11**, 1119240.
4 M. A. Esteso and C. M. Romero, *Int. J. Mol. Sci.*, 2024, **25**, 4547.
5 Y. Wu, S. Aslani, H. Han, C. Tang, G. Wu, X. Li, H. Wu, C. L. Stern, Q.-H. Guo, Y. Qiu, A. X. Y. Chen, Y. Jiao, R. Zhang, A. H. G. David, D. W. Armstrong and J. Fraser Stoddart, *Nat. Synth.*, 2024, **3**, 698–706.
6 G. Crini, *Chem. Rev.*, 2014, **114**, 10940–10975.
7 R. Kumar, A. Sharma, H. Singh, P. Suating, H. S. Kim, K. Sunwoo, I. Shim, B. C. Gibb and J. S. Kim, *Chem. Rev.*, 2019, **119**, 9657–9721.
8 Y. C. Pan, X. Y. Hu and D. S. Guo, *Angew. Chem., Int. Ed.*, 2020, **60**, 2768–2794.

9 W. Y. Yi, F. L. Supian, M. Musa, N. F. N. Abd Karim and A. F. Naim, *Macromol. Res.*, 2022, **30**, 853–862.
10 F.-Y. Chen, W.-C. Geng, K. Cai and D.-S. Guo, *Chin. Chem. Lett.*, 2024, **35**, 109161.
11 X. W. Xu, X. L. Wang, A. M. Wu, Z. M. Zheng, M. G. Yi and R. Xiao, *J. Heterocycl. Chem.*, 2009, **46**, 1137–1141.
12 P. Wang, Y. Li, L. Zhao, Y. Yang, X. Kang, T. Yang, F. Cao, L. Cheng and L. Cao, *Chin. J. Chem.*, 2025, **43**, 1173–1180.
13 P. G. Ghasemabadi, T. Yao and G. J. Bodwell, *Chem. Soc. Rev.*, 2015, **44**, 6494–6518.
14 C. J. Brown and A. C. Farthing, *Nature*, 1949, **164**, 915–916.
15 D. J. Cram and H. Steinberg, *J. Am. Chem. Soc.*, 1952, **73**, 5691–5704.
16 Z. Liu, S. K. M. Nalluri and J. F. Stoddart, *Chem. Soc. Rev.*, 2017, **46**, 2459–2478.
17 S. Kotha, M. E. Shirbhate and G. T. Waghule, *Beilstein J. Org. Chem.*, 2015, **11**, 1274–1331.
18 Y. Bai, Y. Su, J. Li, B. Yang and Z. Shi, *Sci. China, Ser. B: Chem.*, 2005, **48**, 65–69.
19 D. Yang, L. Arifhodzic, C. R. Ganellin and D. H. Jenkinson, *Eur. J. Med. Chem.*, 2013, **63**, 907–923.
20 E. J. Dale, N. A. Vermeulen, M. Juríček, J. C. Barnes, R. M. Young, M. R. Wasielewski and J. F. Stoddart, *Acc. Chem. Res.*, 2016, **49**, 262–273.
21 I. Neira, A. Blanco-Gómez, J. M. Quintela, M. D. García and C. Peinador, *Acc. Chem. Res.*, 2020, **53**, 2336–2346.
22 G. P. Moss, *Pure Appl. Chem.*, 1996, **68**, 2193–2222.
23 J. S. Kandula, V. P. K. Rayala and R. Pullapanthula, *Sep. Sci. Plus*, 2023, **6**, 2200131.
24 J. R. Brandt, F. Salerno and M. J. Fuchter, *Nat. Rev. Chem.*, 2017, **1**, 0045.
25 J. J. Pelayo, I. Valencia, A. P. García, L. Chang, M. López, D. Toffoli, M. Stener, A. Fortunelli and I. L. Garzón, *Adv. Phys.:X*, 2018, **3**, 1509727.
26 F. Devínsky, *Symmetry*, 2021, **13**, 2277.
27 P. Peluso and B. Chankvetadze, *Chem. Rev.*, 2022, **122**, 13235–13400.
28 N. Berova, G. Pescitelli, A. G. Petrovic and G. Proni, *Chem. Commun.*, 2009, 5958–5980.
29 C. Wolf and K. W. Bentley, *Chem. Soc. Rev.*, 2013, **42**, 5408.
30 M. Quan, X. Y. Pang and W. Jiang, *Angew. Chem., Int. Ed.*, 2022, **61**, e202201258.
31 G. Longhi, E. Castiglioni, J. Koshoubu, G. Mazzeo and S. Abbate, *Chirality*, 2016, **28**, 696–707.
32 W.-L. Zhao, M. Li, H.-Y. Lu and C.-F. Chen, *Chem. Commun.*, 2019, **55**, 13793–13803.
33 L. A. P. Kane-Maguire and G. G. Wallace, *Chem. Soc. Rev.*, 2010, **39**, 2545–2576.
34 M. Zhang, G. Qing and T. Sun, *Chem. Soc. Rev.*, 2012, **41**, 1972–1984.
35 Y. Wang, J. Xu, Y. Wang and H. Chen, *Chem. Soc. Rev.*, 2013, **42**, 2930–2962.
36 Z. Lv, Z. Chen, K. Shao, G. Qing and T. Sun, *Polymers*, 2016, **8**, 310.
37 M.-L. Li, J.-B. Pan and Q.-L. Zhou, *Nat. Catal.*, 2022, **5**, 571–577.
38 C. Hao, C. Xu and H. Kuang, *Chem. Commun.*, 2023, **59**, 12959–12971.
39 E. Sanganyado, Z. Lu, Q. Fu, D. Schlenk and J. Gan, *Water Res.*, 2017, **124**, 527–542.
40 Y. Teng, C. Gu, Z. Chen, H. Jiang, Y. Xiong, D. Liu and D. Xiao, *Chirality*, 2022, **34**, 1094–1119.
41 T. Geng, B. Cui, N. Bu, Z. Yan, J. Fan, J. Lu, Y. Fu, Y. Yuan, N. Gao and L. Xia, *J. Phys. Chem. C*, 2023, **127**, 18718–18726.
42 S. Jia, T. Tao, Y. Xie, L. Yu, X. Kang, Y. Zhang, W. Tang and J. Gong, *Small*, 2023, **20**, 2307874.
43 G. Liu, M. G. Humphrey, C. Zhang and Y. Zhao, *Chem. Soc. Rev.*, 2023, **52**, 4443–4487.
44 R. Fu, Q. Y. Zhao, H. Han, W. L. Li, F. Y. Chen, C. Tang, W. Zhang, S. D. Guo, D. Y. Li, W. C. Geng, D. S. Guo and K. Cai, *Angew. Chem., Int. Ed.*, 2023, **62**, e202315990.
45 X. Yang and W. Jiang, *J. Am. Chem. Soc.*, 2024, **146**, 3900–3909.
46 L. Pu, *Acc. Chem. Res.*, 2011, **45**, 150–163.
47 L. Pu, *Chem. Rev.*, 2024, **124**, 6643–6689.
48 T. Kawase, T. Nakamura, K. Utsumi, K. Matsumoto, H. Kurata and M. Oda, *Chem.–Asian J.*, 2008, **3**, 573–577.
49 F. Diederich, M. R. Hester and M. A. Uyeki, *Angew. Chem., Int. Ed.*, 1988, **27**, 1705–1711.
50 P. P. Castro, T. M. Georgiadis and F. Diederich, *J. Org. Chem.*, 1989, **54**, 5835–5838.
51 J. A. Gavin, N. L. Deng, M. Alcala and T. E. Mallouk, *Chem. Mater.*, 1998, **10**, 1937–1944.
52 P. Rajakumar, K. Sekar and K. Srinivasan, *Tetrahedron Lett.*, 2005, **46**, 1905–1907.
53 P. Rajakumar, R. Raja, S. Selvam, R. Rengasamy and S. Nagaraj, *Bioorg. Med. Chem. Lett.*, 2009, **19**, 3466–3470.
54 P. Rajakumar, K. Sekar, V. Shanmugaiah and N. Mathivanan, *Eur. J. Med. Chem.*, 2009, **44**, 3040–3045.
55 Q.-S. Lu, J. Zhang, L. Jiang, J.-T. Hou and X.-Q. Yu, *Tetrahedron Lett.*, 2010, **51**, 4395–4399.
56 K. Takaishi, S. Murakami, F. Yoshinami and T. Ema, *Angew. Chem., Int. Ed.*, 2022, **61**, e202204609.
57 K. Takaishi, F. Yoshinami, Y. Sato and T. Ema, *Chem.–Eur. J.*, 2024, **30**, e202400866.
58 A. Garci, S. Abid, A. H. G. David, M. D. Codesal, L. Đorđević, R. M. Young, H. Sai, L. Le Bras, A. Perrier, M. Ovalle, P. J. Brown, C. L. Stern, A. G. Campaña, S. I. Stupp, M. R. Wasielewski, V. Blanco and J. F. Stoddart, *Angew. Chem., Int. Ed.*, 2022, **61**, e202208679.
59 R. Matsuda, H. Otake, K. Sato and K. Kinbara, *Polym. J.*, 2023, **55**, 1225–1229.
60 I. Solymosi, S. Krishna, E. Nuin, H. Maid, B. Scholz, D. M. Guldi, M. E. Pérez-Ojeda and A. Hirsch, *Chem. Sci.*, 2021, **12**, 15491–15502.
61 P. Spenst and F. Würthner, *Angew. Chem., Int. Ed.*, 2015, **54**, 10165–10168.
62 M. Sapotta, P. Spenst, C. R. Saha-Möller and F. Würthner, *Org. Chem. Front.*, 2019, **6**, 892–899.
63 M. Weh, K. Shoyama and F. Würthner, *Nat. Commun.*, 2023, **14**, 243.
64 G. Ouyang, J. Rühe, Y. Zhang, M. J. Lin, M. Liu and F. Würthner, *Angew. Chem., Int. Ed.*, 2022, **61**, e202206706.

65 T. Türel, S. Bhargava and S. Valiyaveettil, *J. Org. Chem.*, 2020, **85**, 3092–3100.
66 S. E. Penty, M. A. Zwijnenburg, G. R. F. Orton, P. Stachelek, R. Pal, Y. Xie, S. L. Griffin and T. A. Barendt, *J. Am. Chem. Soc.*, 2022, **144**, 12290–12298.
67 A. Yeung, M. A. Zwijnenburg, G. R. F. Orton, J. H. Robertson and T. A. Barendt, *Chem. Sci.*, 2024, **15**, 5516–5524.
68 M. Weh, J. Rühe, B. Herbert, A. M. Krause and F. Würthner, *Angew. Chem., Int. Ed.*, 2021, **60**, 15323–15327.
69 M. Weh, A. A. Kroeger, K. Shoyama, M. Grüne, A. Karton and F. Würthner, *Angew. Chem., Int. Ed.*, 2023, **62**, e202301301.
70 D. P. Sukumaran, K. Shoyama, R. K. Dubey and F. Würthner, *J. Am. Chem. Soc.*, 2024, **146**, 22077–22084.
71 F. Zhao, J. Zhao, H. Liu, Y. Wang, J. Duan, C. Li, J. Di, N. Zhang, X. Zheng and P. Chen, *J. Am. Chem. Soc.*, 2023, **145**, 10092–10103.
72 Y. Shi, C. Li, J. Di, Y. Xue, Y. Jia, J. Duan, X. Hu, Y. Tian, Y. Li, C. Sun, N. Zhang, Y. Xiong, T. Jin and P. Chen, *Angew. Chem., Int. Ed.*, 2024, **63**, e202402800.
73 J. I. Kikuchi, T. Ogata, M. Inada and Y. Murakami, *Chem. Lett.*, 1996, **25**, 771–772.
74 J. S. You, X. Q. Yu, G. L. Zhang, Q. X. Xiang, J. B. Lan and R. G. Xie, *Chem. Commun.*, 2001, 1816–1817.
75 S.-J. Guo, K. Luo, W.-H. Wang, S.-Y. Zhang, H.-Y. Jiang, J.-B. Lan and R.-G. Xie, *Chem. J. Chin. Univ.-Chin.*, 2006, **27**, 1664–1668.
76 X. Huang, A. Hao and P. Xing, *Chem. Mater.*, 2024, **36**, 10361–10370.
77 J. M. Coteron, C. Vicent, C. Bosso and S. Penades, *J. Am. Chem. Soc.*, 1993, **115**, 10066–10076.
78 J. C. Morales and S. Penadés, *Tetrahedron Lett.*, 1996, **37**, 5011–5014.
79 P. V. Murphy, *Eur. J. Org Chem.*, 2007, **2007**, 4177–4187.
80 D. Doyle and P. V. Murphy, *Carbohydr. Res.*, 2008, **343**, 2535–2544.
81 R. Leyden, T. Velasco-Torrijos, S. André, S. Gouin, H.-J. Gabius and P. V. Murphy, *J. Org. Chem.*, 2009, **74**, 9010–9026.
82 D. V. Jarikote and P. V. Murphy, *Eur. J. Org Chem.*, 2010, **2010**, 4959–4970.
83 P. Murphy, S. André and H.-J. Gabius, *Molecules*, 2013, **18**, 4026–4053.
84 S. Bazzi, A. Hadj Mohamed, D. Ryzhakov, J. Ghouilem, M. A. Beniddir, V. Gandon and S. Messaoudi, *Angew. Chem., Int. Ed.*, 2024, **64**, e202418057.
85 Y. Wu, M. Frasconi, D. M. Gardner, P. R. McGonigal, S. T. Schneebeli, M. R. Wasielewski and J. F. Stoddart, *Angew. Chem., Int. Ed.*, 2014, **53**, 9476–9481.
86 D. Deb, M. Parashar, S. Sarkar, S. Ghosh, S. Balasubramanian and S. J. George, *Angew. Chem., Int. Ed.*, 2025, e20385.
87 K. Tanabe, N. Hisano and T. Haino, *Asian J. Org. Chem.*, 2025, **14**, e00251.
88 P. L. Ang, V. H. Nguyen and J. H. K. Yip, *Dalton Trans.*, 2021, **50**, 11422–11428.
89 C. Kind, M. Reiher, J. Röder and B. A. Hess, *Phys. Chem. Chem. Phys.*, 2000, **2**, 2205–2210.
90 D. Cao, H. Kolshorn and H. Meier, *Tetrahedron Lett.*, 1995, **36**, 7069–7072.
91 M. S. Brody, R. M. Williams and M. G. Finn, *J. Am. Chem. Soc.*, 1997, **119**, 3429–3433.
92 S. Thorand, F. Vögtle and N. Krause, *Angew. Chem., Int. Ed.*, 1999, **38**, 3721–3723.
93 M. D. Clay and A. G. Fallis, *Angew. Chem., Int. Ed.*, 2005, **44**, 4039–4042.
94 M. Leclère and A. G. Fallis, *Angew. Chem., Int. Ed.*, 2007, **47**, 568–572.
95 I. R. Lahoz, A. Navarro-Vázquez, A. L. Llamas-Saiz, J. L. Alonso-Gómez and M. M. Cid, *Chem.–Eur. J*, 2012, **18**, 13836–13843.
96 I. R. Lahoz, S. Castro-Fernandez, A. Navarro-Vazquez, J. Lorenzo Alonso-Gomez and M. Magdalena Cid, *Chirality*, 2014, **26**, 563–573.
97 S. Castro-Fernández, J. Álvarez-García, L. García-Río, C. Silva-López and M. M. Cid, *Org. Lett.*, 2019, **21**, 5898–5902.
98 J. Álvarez-García, V. Rubio-Pisabarro, L. García-Río and M. Magdalena Cid, *Org. Chem. Front.*, 2023, **10**, 5435–5442.
99 T. He, M. Huo, P. Wang, H. Huo, T. Yang, F. Cao, L. Zhao, Y. Yang, L. Cheng and L. Cao, *Angew. Chem., Int. Ed.*, 2025, **64**, e202516534.
100 H. Kawashima, D. Tauchi, M. Sakura, K. Tsubaki and M. Hasegawa, *Chem.–Asian J.*, 2025, **20**, e202401920.
101 K. Utsumi, T. Kawase and M. Oda, *Chem. Lett.*, 2003, **32**, 412–413.
102 T. Kawase, Y. Daifuku, Y. Hirao, K. Matsumoto, H. Kurata and T. Kubo, *C. R. Chim.*, 2009, **12**, 403–411.
103 D. Meidlinger, L. Marx, C. Bordeianu, S. Choppin, F. Colobert and A. Speicher, *Angew. Chem., Int. Ed.*, 2018, **57**, 9160–9164.
104 L. Marx, D. Lamberty, S. Choppin, F. Colobert and A. Speicher, *Eur. J. Org Chem.*, 2021, **2021**, 1351–1354.
105 Y. Li, A. Yagi and K. Itami, *J. Am. Chem. Soc.*, 2020, **142**, 3246–3253.
106 T. Furo, T. Mori and Y. Inoue, *Chirality*, 2010, **22**, E17–E21.
107 O. R. P. David, *Tetrahedron*, 2012, **68**, 8977–8993.
108 Z. Hassan, *Adv. Funct. Mater.*, 2024, **34**, 2311828.
109 X. Zhang, Y. Zhou, Z. X. Yu, C. H. Tung and Z. Xu, *Angew. Chem., Int. Ed.*, 2025, **64**, e202420667.
110 J. Seibert, Y. Xu, H. Hafeez, J. Podlech, L. Favereau, E. Spuling, C. Waldhelm, M. Nieger, O. Fuhr, Z. Hassan, J. Crassous, I. D. W. Samuel, E. Zysman-Colman and S. Bräse, *Adv. Funct. Mater.*, 2024, **34**, 2401956.
111 M. R. Rapp, W. Leis, F. Zinna, L. Di Bari, T. Arnold, B. Speiser, M. Seitz and H. F. Bettinger, *Chem.–Eur. J*, 2022, **28**, e202104161.
112 Y. Morisaki, M. Gon, T. Sasamori, N. Tokitoh and Y. Chujo, *J. Am. Chem. Soc.*, 2014, **136**, 3350–3353.
113 Y. Morisaki, K. Inoshita and Y. Chujo, *Chem.–Eur. J*, 2014, **20**, 8386–8390.
114 A. Morisaki, R. Inoue and Y. Morisaki, *Chem.–Eur. J*, 2023, **29**, e202203533.

115 E. Sidler, P. Zwick, C. Kress, K. Reznikova, O. Fuhr, D. Fenske and M. Mayor, *Chem.–Eur. J*, 2022, **28**, e202201764.
116 M. Hasegawa, Y. Ishida, H. Sasaki, S. Ishioka, K. Usui, N. Hara, M. Kitahara, Y. Imai and Y. Mazaki, *Chem.–Eur. J*, 2021, **27**, 16225–16231.
117 N. Miki, R. Inoue and Y. Morisaki, *Bull. Chem. Soc. Jpn.*, 2022, **95**, 110–115.
118 E. Kumamoto, N. Miki, R. Inoue and Y. Morisaki, *ChemPlusChem*, 2025, e202500276.
119 S. Gabutti, S. Schaffner, M. Neuburger, M. Fischer, G. Schaefer and M. Mayor, *Org. Biomol. Chem.*, 2009, **7**, 3222–3229.
120 S. K. Keshri, A. Takai, T. Ishizuka, T. Kojima and M. Takeuchi, *Angew. Chem., Int. Ed.*, 2020, **59**, 5254–5258.
121 K. Tani, Y. Tohda, H. Takemura, H. Ohkita, S. Ito and M. Yamamoto, *Chem. Commun.*, 2001, 1914–1915.
122 K. Tani, R. Imafuku, K. Miyanaga, M. E. Masaki, H. Kato, K. Hori, K. Kubono, M. Taneda, T. Harada, K. Goto, F. Tani and T. Mori, *J. Phys. Chem. A*, 2020, **124**, 2057–2063.
123 Y. Kawai, J. Nogami, Y. Nagashima and K. Tanaka, *Chem. Sci.*, 2023, **14**, 3963–3972.
124 L. Chen, X. Liang, P. Wang, L. Fang, D. Zhou, K. Li, W. Wu and C. Yang, *Angew. Chem., Int. Ed.*, 2025, **64**, e21400.
125 Y. Ishida, E. Iwasa, Y. Matsuoka, H. Miyauchi and K. Saigo, *Chem. Commun.*, 2009, 3401–3403.
126 G. Yang and J. Wang, *Angew. Chem., Int. Ed.*, 2024, e202412805.
127 L. Yang, Y. P. Zhang, Y. You, Z. H. Wang, W. C. Yuan and J. Q. Zhao, *Chem. Rec.*, 2025, **25**, e202500085.
128 J. Wang, K. Lv, Y. Wen, T. Liu and C. Zhao, *Nat. Commun.*, 2025, **16**, 3170.
129 S. Wei, L.-Y. Chen and J. Li, *ACS Catal.*, 2023, **13**, 7450–7456.
130 S. Zhang, Y. Wei, Q. Chen, Y. Qian, G. Wu, C. Ge, F. Huang and H. Li, *J. Am. Chem. Soc.*, 2025, **147**, 36843–36850.
131 C. Tang, R. Zhang, S. Almunif, P. J. Das, P. J. Brown, R. M. Young, G. Wu, H. Han, X. Zhao, A. H. G. David, H. Wu, B. Song, A. Abhervé, Y. Wu, Y.-M. Ye, Y. Feng, A. X. Y. Chen, C. L. Stern, Z. Li, E. A. Scott, M. R. Wasielewski and J. F. Stoddart, *Nat. Synth.*, 2025, **4**, 956–964.
132 K.-i. Sugiura, *Front. Chem.*, 2020, **8**, 700.
133 D. T. Longone and H. S. Chow, *J. Am. Chem. Soc.*, 1964, **86**, 3898–3899.
134 D. T. Longone and H. S. Chow, *J. Am. Chem. Soc.*, 1970, **92**, 994–998.
135 M. Nakazaki, K. Yamamoto, S. Tanaka and H. Kametani, *J. Org. Chem.*, 1977, **42**, 287–291.
136 S. Misumi and T. Otsubo, *Acc. Chem. Res.*, 1978, **11**, 251–256.
137 R. Katoono, Y. Obara, K. Fujiwara and T. Suzuki, *Chem. Sci.*, 2018, **9**, 2222–2229.
138 R. Katoono and K. Shimomura, *Chem. Commun.*, 2022, **58**, 13385–13388.
139 L. Zhao, L. Cheng, Y. Yang, P. Wang, P. Tian, T. Yang, H. Nian and L. Cao, *Angew. Chem., Int. Ed.*, 2024, **63**, e202405150.
140 G. Sun, X. Zhang, Z. Zheng, Z.-Y. Zhang, M. Dong, J. L. Sessler and C. Li, *J. Am. Chem. Soc.*, 2024, **146**, 26233–26242.
141 X. Zhang, C.-C. Shen, R. Tan, Z.-Y. Zhang, Y.-Y. Zhang, Y.-H. Liu, W.-T. Wu, A.-T. Hu, T.-Y. Dong, K.-Y. Zheng, H. Min, J. Li, M. Dong, Y. Zhang and C. Li, *Org. Lett.*, 2025, **27**, 9820–9824.
142 X. Xie, F. Zhang, H. Qin, X. Lu, B. Zhang and Q. Sun, *Inorg. Chem. Commun.*, 2023, **156**, 111303.
143 M. Busch, M. Cayir, M. Nieger, W. R. Thiel and S. Bräse, *Eur. J. Org Chem.*, 2013, **2013**, 6108–6123.
144 N. Takenaga, S. Adachi, A. Furusawa, K. Nakamura, N. Suzuki, Y. Ohta, M. Komizu, C. Mukai and S. Kitagaki, *Tetrahedron*, 2016, **72**, 6892–6897.
145 S. V. Kumar and P. J. Guiry, *Angew. Chem., Int. Ed.*, 2022, **61**, e202205516.
146 W. Guo, J. Jiang and J. Wang, *Angew. Chem., Int. Ed.*, 2024, **63**, e202400279.
147 N. Sharma, E. Spuling, C. M. Mattern, W. Li, O. Fuhr, Y. Tsuchiya, C. Adachi, S. Bräse, I. D. W. Samuel and E. Zysman-Colman, *Chem. Sci.*, 2019, **10**, 6689–6696.
148 L. Chen, C. Li, Z.-F. Liu, Y. Kuboi, E. Fu, L. S. Vargas, C. Adachi, F. Mathevet and S. Zhang, *Chem. Commun.*, 2024, **60**, 1758–1761.
149 S. E. Penty, G. R. F. Orton, D. J. Black, R. Pal, M. A. Zwijnenburg and T. A. Barendt, *J. Am. Chem. Soc.*, 2024, **146**, 5470–5479.
150 S. E. Penty, M. V. Appleby, M. A. Zwijnenburg, D. J. Black, D. Hartmann, D. Chekulaev, J. Weinstein, R. Pal and T. A. Barendt, *Chem.–Eur. J*, 2025, **31**, e01734.
151 D. Hartmann, S. E. Penty, M. A. Zwijnenburg, R. Pal and T. A. Barendt, *Angew. Chem., Int. Ed.*, 2025, **64**, e202501122.
152 L. T. Bao, R. H. Zhang, X. Yuan, X. Wang, P. Wu, X. Q. Wang, J. Chen, A. Zhu, H. B. Yang and W. Wang, *Angew. Chem., Int. Ed.*, 2025, **64**, e202500472.
153 M. Shimada, Y. Yamanoi, T. Ohto, S.-T. Pham, R. Yamada, H. Tada, K. Omoto, S. Tashiro, M. Shionoya, M. Hattori, K. Jimura, S. Hayashi, H. Koike, M. Iwamura, K. Nozaki and H. Nishihara, *J. Am. Chem. Soc.*, 2017, **139**, 11214–11221.
154 Z. Wang, Y. Liu, X. Quan, W. Zhang, R. Tan, H. Gu, C. Sheng, C. Duan, P. Xing and J. H. Wan, *Angew. Chem., Int. Ed.*, 2024, **64**, e202413295.